



# 1 Using spectra characteristics to identify ice nucleating particle 2 populations during winter storms in the Alps

3 Jessie M. Creamean<sup>1,2\*</sup>, Claudia Mignani<sup>3</sup>, Nicolas Bukowiecki<sup>4</sup>, Franz Conen<sup>3</sup>

4 <sup>1</sup>Cooperative Institute for Research in Environmental Sciences, University of Colorado, Boulder, CO, USA

5 <sup>2</sup>Physical Sciences Division, National Oceanic and Atmospheric Administration, Boulder, CO, USA

6 <sup>3</sup>Department of Environmental Sciences, University of Basel, Switzerland

7 <sup>4</sup>Laboratory of Atmospheric Chemistry, Paul Scherrer Institute, Villigen, Switzerland

8 \*Now at: Department of Atmospheric Science, Colorado State University, Fort Collins, CO, USA

9

10 Email: [jessie.creamean@colostate.edu](mailto:jessie.creamean@colostate.edu)

11

12 **Abstract.** One of the least understood cloud processes is modulation of their microphysics by aerosols, specifically of cloud ice  
13 by ice nucleating particles (INPs). To investigate INP impacts on cloud ice and subsequent precipitation formation, measurements  
14 in cloud environments are necessary but difficult given the logistical challenges associated with airborne measurements and  
15 separating interstitial aerosol from cloud residues. Additionally, determining the sources of INPs is important given the dependency  
16 of glaciation temperatures on the mineral or biological components and diversity of such INP populations. Here, we present results  
17 from a comparison of INP spectral characteristics in air, cloud rime, and fresh fallen snow for storm days at the High-Altitude  
18 Research Station, Jungfraujoch. The goal of the study was two-fold: (1) to assess variability in wintertime INP populations found  
19 in-cloud based on air mass direction during snowfall and (2) to evaluate INPs between different sample types using normalized  
20 differential INP spectra. INP freezing temperatures and concentrations were consistently higher on average from the southeast as  
21 compared to the northwest for rime, snow and especially aerosol samples which is likely a result of air mass influence from  
22 boundary layer terrestrial and marine sources in Southern Europe, the Mediterranean, and North Africa. For all three sample types  
23 combined, average onset freezing temperatures were  $-7.7$  and  $-12$  °C for southeasterly and northwesterly days, respectively, while  
24 INP concentrations were 3 to 20 times higher when winds arrived from the southeast. Southeasterly aerosol samples typically had  
25 bimodal freezing spectra—indicating a putative influence from biological sources—while bimodality of the rime and snow varied  
26 depending on meteorological context. Evaluating normalized differential INP spectra exhibited variable modality and shape—  
27 depending on the types of INPs present—and may serve as a viable method for comparing different sampling substances and  
28 assessing the possible mixed mineral and biological versus only biological contributions to INP sample populations.

## 29 1 Introduction

30 Aerosols are key players in the atmospheric radiation budget, cloud microphysics, and precipitation development. However, one  
31 of the most significant challenges with regard to aerosols is quantifying their impacts on cloud ice formation through serving as  
32 ice nucleating particles (INPs) (Boucher et al., 2013). Aerosol-induced ice microphysical modifications influence cloud lifetime  
33 and albedo (Albrecht, 1989; Twomey, 1977; Storelvmo et al., 2011), as well as the production of precipitation in clouds containing  
34 both liquid and ice. Mixed-phase clouds (MPCs) are ubiquitous in the troposphere over the entire annual cycle yet are difficult to  
35 quantify globally in part due to an inadequate understanding of aerosol-cloud interactions in mixed-phase environments (Korolev  
36 et al., 2017). Thus, a close evaluation of aerosol-cloud processes is crucial to evaluating weather and climate processes; however,  
37 constraining aerosol-cloud impacts in models, specifically when parameterizing INPs in MPC systems, remains a significant  
38 challenge due to limited observations (Cziczo et al., 2017; Coluzza et al., 2017; DeMott et al., 2010; Kanji et al., 2017; Korolev et  
39 al., 2017). Observations directly in cloudy environments are even more scarce—given the logistical costs and resources required



40 by airborne platforms, caveats associated with aircraft probes and instrumentation, and instrumental artefacts caused by flying  
41 through clouds at high speeds (Cziczo et al., 2017)—but are necessary to assess the impacts of INPs on MPC microphysics as  
42 compared to most surface measurements which are geared towards evaluation of INP sources.

43 In the absence of conditions with  $-38\text{ }^{\circ}\text{C}$  and relative humidity with respect to ice above 140%, INPs are required for initiation of  
44 tropospheric cloud ice formation (Kanji et al., 2017). Aerosols such as dust and primary biological aerosol particles (PBAPs) are  
45 some of the most abundant and efficient INPs found in the atmosphere, respectively (Murray et al., 2012; Hoose and Möhler, 2012;  
46 DeMott et al., 1999; Conen et al., 2011; Creamean et al., 2013). PBAPs originating from certain bacteria, pollens, and vegetative  
47 detritus are the most efficient INPs known, capable of initiating freezing near  $-1\text{ }^{\circ}\text{C}$ , while most PBAPs (e.g., fungal spores, algae,  
48 and diatoms) tend to nucleate ice at temperatures similar to those of mineral dust (Despres et al., 2012; Murray et al., 2012; Tobo  
49 et al., 2014; Hader et al., 2014a; O'Sullivan et al., 2014; Hill et al., 2016; Tesson et al., 2016; Alpert et al., 2011; Knopf et al., 2010;  
50 Fröhlich-Nowoisky et al., 2015). In general, previous works collectively indicate that PBAP INPs that nucleate ice greater than  
51 approximately  $-10\text{ }^{\circ}\text{C}$  are bacterial (Murray et al., 2012; Hu et al., 2018; Hoose and Möhler, 2012; Despres et al., 2012; Fröhlich-  
52 Nowoisky et al., 2016), but could also be pollen or certain fungal spores (von Blohn et al., 2005; Hoose and Möhler, 2012;  
53 O'Sullivan et al., 2016), although the latter two are less likely. Plant bacteria such as *Pseudomonas syringae* are deemed  
54 omnipresent in the atmosphere and precipitation (Despres et al., 2012; Stopelli et al., 2017; Morris et al., 2014), and facilitate cloud  
55 ice formation up to  $-1\text{ }^{\circ}\text{C}$  (Despres et al., 2012). While, only a few laboratory-based studies have reported known inorganic or  
56 mineral materials that ice nucleation activity at such temperatures (Ganguly et al., 2018; Atkinson et al., 2013). Mineral and soil  
57 dust serving as atmospheric shuttles for organic microbial fragments can be transported thousands of kilometres and serve as  
58 effective INPs, even from highly arid regions such as the Sahara (Kellogg and Griffin, 2006), yet the exact origin of the ice  
59 nucleation germ forming at the warmest temperatures is speculated to be due to the ice binding proteins or macromolecules of the  
60 biological components (O'Sullivan et al., 2014; O'Sullivan et al., 2016; Conen and Yakutin, 2018). In general, the previous studies  
61 on the climate relevance of PBAPs demonstrate the importance of such INPs at MPC temperatures and precipitation enhancement  
62 (Morris et al., 2004; Bergeron, 1935; Christner et al., 2008; Morris et al., 2014; Morris et al., 2017; Stopelli et al., 2014; Fröhlich-  
63 Nowoisky et al., 2016).

64 Although biological constituents, from cellular material to in-tact bacteria and spores, are thought to be omnipresent in the  
65 atmosphere (Burrows et al., 2009b; Burrows et al., 2009a; Jaenicke, 2005; Jaenicke et al., 2007), modeling studies constraining  
66 global emission estimates of biological INPs and PBAPs are very limited, subject to significant hurdles, and often yield conflicting  
67 results due to the dearth of observations and complexity of atmospheric PBAPs (Hummel et al., 2015; Burrows et al., 2013; Twohy  
68 et al., 2016; Fröhlich-Nowoisky et al., 2012; Despres et al., 2012; Hoose and Möhler, 2012; Morris et al., 2011). Yet, biological  
69 aerosols such as bacteria have been shown to cause significant perturbations in cloud ice in numerical weather prediction models,  
70 affording modulations in cloud radiative forcing and precipitation formation (Sahyoun et al., 2017). In addition, measuring and  
71 quantifying PBAPs is non-trivial—methodologies for counting, culturing, and nucleic acid sequencing of PBAPs and especially  
72 for those which fall in the warm temperature INP regime (i.e., INPs that nucleate ice  $> -15\text{ }^{\circ}\text{C}$ ) are: (1) time and labor intensive,  
73 (2) require specific expertise or at times substantial resources, (3) require substantial sample volumes, or (4) are species- or genera-  
74 specific or limited to viable microorganisms (Despres et al., 2012). Although such techniques are required to adequately assess the  
75 atmospheric microbiome and PBAP sources, a simpler approach could be applied to evaluate and even quantify warm temperature  
76 biological INP populations as compared to colder temperature PBAPs or mineral dust.



77 The goal of the study presented here focuses on: (1) an intercomparison of INP measurements of aerosol, cloud rime, and snow  
78 directly in cloudy environments at the ground and (2) evaluating INP spectra in a manner such that we can estimate the relative  
79 contribution from biological INPs in the warm temperature regime relevant to MPCs. Sampling was conducted at the High-Altitude  
80 Research Station Jungfrauoch (JFJ), a unique location for evaluating populations of INPs that affect winter storms in the European  
81 Alps, and where MPCs are particularly common (Lohmann et al., 2016). Recent studies at JFJ have provided valuable insight into  
82 INP concentrations, sources, and removal processes under a variety of conditions and during various times of the year. Conen et  
83 al. (2015) measured INPs at  $-8\text{ }^{\circ}\text{C}$  over the course of a year at JFJ, and found a strong seasonality in such INPs, with two order of  
84 magnitude higher concentrations observed during the summer. They also suggested INPs measured at this temperature may be  
85 limited most of the year by microphysical processing during transit. Stopelli et al. (2015) verified this removal mechanistic process  
86 through INP measurements and isotopic composition of fresh fallen snow at JFJ, concluding that warm temperature (i.e., INPs  
87 active at  $> -10\text{ }^{\circ}\text{C}$ ) are rapidly depleted by precipitating clouds at lower elevations. Stopelli et al. (2016) expanded their INP  
88 analyses to 2-years of data at JFJ, concluding that a high abundance of INPs at  $-8\text{ }^{\circ}\text{C}$  is to be expected whenever high wind speed  
89 coincides with air masses having experienced little or no precipitation prior to sampling, yet a separate study by Stopelli et al.  
90 (2017) found that only a small fraction of the INPs were bacterial cells. In contrast, Lacher et al. (2018a; 2018b) conducted an  
91 interannual synopsis of INP measurements at JFJ and found anthropogenic influence on INP concentrations, but only during  
92 boundary layer influences and at relatively cold temperatures (i.e., approximately  $-30\text{ }^{\circ}\text{C}$ ), and higher INP concentrations during  
93 Saharan dust events (SDEs) and marine boundary layer air arriving at JFJ. Eriksen Hammer et al. (2018) characterized ice particle  
94 residuals and concluded that silica and aluminosilicates were the most important ice particle residuals at JFJ during the mixed-  
95 phase cloud events during Jan – Feb 2017, while carbon-rich particles of possible biological origin were of minor contribution.

96 Here, we demonstrate how variable sources influence INP populations depending on air mass transport and storm direction, and  
97 spectral modality between the rime, snow, and aerosols can help explain the exchange of INPs from air into cloud then into  
98 precipitation. Our results expand upon previous studies by evaluating INPs via a combination of aerosol, rime, and snow, and at a  
99 temperature range that comprises common biological and mineral INPs.

## 100 2 Methods

### 101 2.1 Aerosol, cloud rime and snow collection at Jungfrauoch

102 Collocated collection of snow, cloud rime, and aerosol samples for Ice Nucleation Characterization in the Alps of Switzerland  
103 (INCAS) study took place 15 Feb – 11 Mar 2018 in the Sphinx observatory at JFJ ( $46.55\text{ }^{\circ}\text{N}$ ,  $7.98\text{ }^{\circ}\text{E}$ ; 3580 m above sea level (m  
104 a.s.l.); <https://www.hfsjg.ch/en/home/>). Snow was collected as described by Stopelli et al. (2015) using a Teflon-coated tin ( $0.1$   
105  $\text{m}^2$ , 8 cm deep) for a duration of 1 – 18 hours, but typically for 1 – 4 hours. Cloud rime was collected using a slotted plexiglass  
106 plate placed vertically during snow sample collection (Lacher et al., 2017; Mignani et al., 2018). Daily size-resolved aerosol  
107 samples were collected using a Davis Rotating-drum Universal-size-cut Monitoring (DRUM) single-jet impactor (DA400,  
108 DRUMAir, LLC.) as described by Creamean et al. (2018a) from a 1-m long inlet constructed of 6.4-mm inner diameter static-  
109 dissipative polyurethane tubing (McMaster-Carr®) leading to outside of the Sphinx and connected to a funnel covered with a loose,  
110 perforated plastic bag to prevent rimed ice build-up or blowing snow from clogging the inlet. The DRUM collected aerosol particles  
111 at four size ranges ( $0.15 - 0.34$ ,  $0.34 - 1.20$ ,  $1.20 - 2.96$ , and  $2.96 - >12\text{ }\mu\text{m}$  in diameter) and sampled at  $27.7\text{ L min}^{-1}$ , equalling  
112 39888 total L of air per sample. Such size ranges cover a wide array of aerosols—particularly those that serve as INPs (DeMott et  
113 al., 2010; Fridlind et al., 2012; Mason et al., 2016)—while the large volume of air collected promotes collection of rarer, warm



114 temperature biological INPs, but may represent a lower fraction of overall INP concentrations (Mossop and Thorndike, 1966).  
115 Samples were deposited onto 20 x 190 mm strips of petrolatum-coated (100%, Vaseline®) perfluoroalkoxy plastic (PFA, 0.05 mm  
116 thick) substrate secured onto the rotating drums (20 mm thick, 60 mm in diameter) in each of the four stages at the rate of 7 mm  
117 per day (5 mm of sample streaked onto the PFA followed by 2 mm of blank).

## 118 2.2 Ice nucleation measurements

119 All samples were analysed immediately after collection for INPs using a drop freezing cold plate system described by Creamean  
120 et al. (2018b). Briefly, snow and cloud rime samples were melted into covered 50-mL glass beakers for analysis, resulting in  
121 approximately 10 mL of liquid per sample. Samples were manually shaken prior to analysis. Aerosols deposited onto the PFA  
122 were prepared for drop freezing by cutting out each daily sample and placing in a 50-mL glass beaker with 2 mL of molecular  
123 biology reagent grade water (Sigma-Aldrich®). Beakers were covered and shaken at 500 rpm for 2 hours (Bowers et al., 2009). In  
124 between sampling, beakers were cleaned with isopropanol (99.5%), sonicated with double-distilled water for 30 minutes, then  
125 heated at 150 °C for 30 minutes.

126 Copper discs (76 mm in diameter, 3.2 mm thick) were prepared by sonicating in double-distilled water for 30 minutes, cleaning  
127 with isopropanol, then coated with a thin layer of petrolatum (Tobo, 2016; Bowers et al., 2009; Polen et al., 2018). Following  
128 sample preparation, a sterile, single-use syringe was used to draw 0.25 mL of the suspension and 100 drops were pipetted onto the  
129 petrolatum-coated copper disc, creating an array of ~2.5-μL aliquots. Drops were visually inspected for size; however, it is possible  
130 not all drops were the same exact volume, which could lead to a small level of indeterminable uncertainty. However, previous  
131 studies have demonstrated that drop size variability within this range does not significantly impact freezing results (Hader et al.,  
132 2014b; Bigg, 1953; Langham and Mason, 1958; Creamean et al., 2018b). The copper disc was then placed on a thermoelectric cold  
133 plate (Aldrich®) and covered with a transparent plastic dome. Small holes in the side of the dome and copper disc permitted  
134 placement of up to four temperature probes using an Omega™ thermometer/data logger (RDXL4SD; 0.1 °C resolution and  
135 accuracy of ± (0.4% + 1 °C) for the K sensor types used). During the test, the cold plate was cooled at 1 – 10 °C min<sup>-1</sup> from room  
136 temperature until around –35 °C. Control experiments at various cooling rates within this range show no discernible dependency  
137 of drop freezing on cooling rate (Creamean et al., 2018b), akin to previous works (Wright and Petters, 2013; Vali and Stansbury,  
138 1966).

139 A +0.33 °C correction factor was added to any temperature herein and an uncertainty of 0.15 °C was added to the probe accuracy  
140 uncertainty based on DFCP characterization testing presented in Creamean et al. (2018b), to account for the temperature difference  
141 between the measurement (i.e., in the plate centre) and actual drop temperature. Frozen drops were detected visually, but recorded  
142 through custom software, providing the freezing temperature and cooling rate of each drop frozen. The test continued until all 100  
143 drops were frozen. Each sample was tested three times with 100 new drops for each test. From each test, the fraction frozen and  
144 percentage of detected frozen drops were calculated (typically, > 90% of the drops were detected). The results from the triplicate  
145 tests were then binned every 0.5 °C to produce one spectrum per sample. Normalized differential INP spectra were created by a  
146 using a combination of calculations. First, cumulative INP spectra were calculated using the equation posed by Vali (1971):

$$147 \quad [INP_S(T)](L^{-1}) = \frac{\ln N_o - \ln N_u(T)}{V_{drop}}$$



148 where  $N_o$  is the total number of drops,  $N_u(T)$  is the number of unfrozen drops at each temperature, and  $V_{drop}$  is the average volume  
149 of each drop. Aerosol INP concentrations were corrected for the total volume of air per sample ( $INPs \times \frac{V_{suspension}}{V_{air}}$ ) while melted  
150 rime/snow residual INPs were adjusted to the total used during analysis ( $INPs \times V_{suspension}$ ), where  $V_{suspension}$  and  $V_{air}$  represent  
151 the total liquid volume analyzed per sample (0.75 mL for the three tests) and total volume of air drawn per sample (39888 L),  
152 respectively. Second, differential values were calculated from each 0.5-°C cumulative concentration bin. Differential INP spectra  
153 were used early in earlier studies (Vali, 1971; Vali and Stansbury, 1966), however, spectra only reached a minimum of -20 °C,  
154 missing the tail end of what are usually the highest INP concentrations as discussed in more detail below. A recent study by Polen  
155 et al. (2018) recommend the use of differential spectra. Third, differential concentrations were divided by the maximum  
156 concentration per sample (i.e., to normalize). Last, spectra were smoothed using a moving average.

### 157 2.3 Supporting meteorological and source analysis data

158 Auxiliary surface meteorological observations, including but not limited to hourly mean air temperature measured 2 m above  
159 ground level (a.g.l.) (°C), relative humidity measured 2 m a.g.l. (%), scalar wind speed ( $\text{m s}^{-1}$ ) and direction (degrees), and incoming  
160 longwave radiation ( $\text{W m}^{-2}$ ) were acquired from MeteoSwiss (<https://gate.meteoswiss.ch/idaweb/>). From the longwave  
161 measurements, in-cloud conditions were determined by calculating the sky temperature and comparing to air temperature measured  
162 at the station, per the methodology of Herrmann et al. (2015) from a 6-year analysis of JFJ observations. For the current work,  
163 each hourly measurement was categorized as out-of-cloud or in-cloud based on such calculations.

164 Radon ( $^{222}\text{Rn}$ ) concentrations have been continuously measured at JFJ since 2009. Details on the detectors themselves and the  
165 measurements can be found in Griffiths et al. (2014). Briefly, 30-minute radon concentrations were measured using a dual-flow-  
166 loop two-filter radon detector as described by Chambers et al. (2016). Calibrated radon concentrations were converted from activity  
167 concentration at ambient conditions to a quantity which is conserved during an air parcel's ascent: activity concentration at standard  
168 temperature and pressure (0 °C, 1013 hPa), written as  $\text{Bq m}^{-3}$  STP (Griffiths et al., 2014). Time periods with boundary layer  
169 intrusion were classified as radon concentrations  $> 2 \text{ Bq m}^{-3}$  (Griffiths et al., 2014). Particle concentrations from approximately  
170 0.3 to  $> 20 \mu\text{m}$  in diameter were measured with a 15-channel optical particle sizer (OPS 3300; TSI, Inc.) at a 1-minute time  
171 resolution (Bukowiecki et al., 2016). Due to operational complications, OPC data were not collected prior to 23 Feb during INCAS.  
172 Air was drawn through a heated total aerosol inlet (25 °C) which, besides aerosol particles, enables hydrometeors with diameters  
173  $< 40 \mu\text{m}$  to enter and to evaporate, at wind speeds of  $20 \text{ m s}^{-1}$  (Weingartner et al., 1999). SDEs were determined from existing  
174 methodology using various aerosol optical properties, but specifically, the Ångström exponent of the single scattering albedo  
175 ( $\tilde{a}_{SSA}$ ), which decreases with wavelength during SDEs (Collaud Coen et al., 2004; Bukowiecki et al., 2016). SDEs are automatically  
176 detected by the occurrence of negative  $\tilde{a}_{SSA}$  that last more than four hours. Most of the SDEs do not lead to a detectable increase  
177 of the 48-h total suspended particulate matter (TSP) concentrations at JFJ. Additionally, we consider these events probable SDEs,  
178 but may have influences from other sources in addition.

179 Air mass transport analyses were conducted using the HYbrid Single Particle Lagrangian Integrated Trajectory model with the  
180 SplitR package for RStudio (<https://github.com/rich-iannone/SplitR>) (Draxler, 1999; Draxler and Rolph, 2011; Stein et al., 2015).  
181 Reanalysis data from the National Centers for Environmental Prediction (NCEP) National Center for Atmospheric Research  
182 (NCAR) (2.5° latitude-longitude; 6-hourly; [https://www.ready.noaa.gov/gbl\\_reanalysis.php](https://www.ready.noaa.gov/gbl_reanalysis.php)) were used as the meteorological fields  
183 in HYSPLIT simulations. Trajectories were initiated at 10, 500, and 1000 m a.g.l. every 3 hours daily. Trajectories were only



184 simulated for each northwesterly and southeasterly case study day (i.e., Table 1). It is important to note that “northwesterly” is a  
185 contribution of north, west, and northwest winds, while “southeasterly” includes south, east, and southeast winds.

### 186 3 Results and discussion

#### 187 3.1 Directional dichotomy of storm systems during INCAS

188 Local surface meteorology was variable at JFJ during INCAS, with air temperatures ranging from  $-27.5$  to  $-4.8$  °C (average of  $-$   
189  $13.7$  °C)—temperatures relevant to heterogeneous nucleation of cloud ice—and relative humidity ranging from 18 to 100% (Figure  
190 1a). Wind speed was  $6.4$  m s $^{-1}$  on average, with spikes during most storm systems up to  $22.8$  m s $^{-1}$  (i.e., wind speed during rime  
191 and snow collection; Figure 1b). Due to the topography surrounding JFJ, predominant wind directions were northwest followed  
192 by southeast, with the fastest winds recorded originating from the southeast (Figure 2). Such conditions are typical for JFJ during  
193 the winter (Stopelli et al., 2015). Out of the entire study, several days were classified as northwesterly or southeasterly during storm  
194 conditions when a combination of aerosol, cloud rime, and snow samples were collected (i.e., a full 24 hours of northwesterly or  
195 a full 24 hours of southeasterly winds during snowfall; Table 1), which are herein focused on as the case study days.

196 Extending past local conditions, air mass transport 10 days back in time prior to reaching JFJ on case study days was, as expected,  
197 dissimilar between northwesterly (Figure 3) and southeasterly (Figure 4) conditions. The main distinctions between northwesterly  
198 and southeasterly days are: (1) northwesterly days originated from farther west, with some days reaching back to the Canadian  
199 Archipelago, while air masses on southeasterly days predominantly hovered over land and occasional oceanic sources closer to  
200 Europe, (2) southeasterly air masses travelled closer to the surface relative to northwesterly days, especially south and east of JFJ  
201 while northwesterly air masses were typically transported from higher altitudes (i.e., more free tropospheric exposure), and (3)  
202 aside from 06 Mar (which is discussed in more detail in the following section), northwesterly air masses did not travel over the  
203 Mediterranean and northern Africa, whereas the southeasterly air masses reaching down to 100 m above JFJ arrived from over  
204 such regions within less than 2 days before arriving to JFJ. Boose et al. (2016) reported similar transport pathways for JFJ during  
205 multiple consecutive winters and concluded that marine and Saharan dust served as dominant sources of INPs. Reche et al. (2018)  
206 also reported similar pathways and sources for bacteria and viruses, but during the summer in southern Spain. Possible SDEs were  
207 automatically detected on 24 Feb and 10 Mar in the current work, and air mass transport pathways are shown for these days. These  
208 disparate sources and transport pathways of air support the variability in the ice nucleation observations as discussed in more detail  
209 in the following section.

210 As evidenced by the air mass transport analyses, each southeasterly case day (and 06 Mar) experienced longer residence times in  
211 what was likely the boundary layer (i.e., 1000 m or less) compared to northwesterly cases, which is supported by  $^{222}\text{Rn}$  data (Figure  
212 5). Griffiths et al. (2014) determined that radon concentrations  $> 2$  Bq m $^{-3}$  signify boundary layer intrusion, which in the current  
213 work was clearly observed on 23 Feb, 06 Mar, and 11 Mar, indicating samples collected on these days were likely influenced by  
214 boundary layer sources (planetary and marine). Relatively low radon concentrations were observed the remaining case study days,  
215 indicating these samples were predominantly affected by free tropospheric air and thus, lower aerosol concentrations and/or more  
216 distant sources. Although OPC data were missing until 23 Feb, source information can be gleaned from the available data. For  
217 example, 23 Feb had episodic high concentrations of particles (maximum of  $9.6$  cm $^{-3}$ ) towards the beginning of the day coincident  
218 with the largest spike in radon, with a steady decrease as time transpired, indicating the boundary layer was an ample source of  $>$   
219  $0.3$   $\mu\text{m}$  particles. Although not a case study time period, a similar correlation between the OPC and radon concentrations was  
220 observed 27 – 28 Feb, where the highest concentrations of each were observed during the entire study time period. Selected days



221 were subject to diurnal upslope winds (Figure 1b), such as 6 Mar, where boundary layer air reached JFJ and a midday maximum  
222 in OPC particle concentrations was observed, indicating lower elevations were the dominant source of aerosol. Although, diurnal  
223 variations in aerosol from local sources have been shown to not be common in the winter at JFJ (Baltensperger et al., 1997). In  
224 contrast, 11 Mar was exposed to boundary layer air based on radon observations, but particle concentrations were low (average of  
225  $0.2 \text{ cm}^{-3}$  compared to a study average of  $3.0 \text{ cm}^{-3}$ ), signifying that although boundary layer intrusion occurred at JFJ, it was not a  
226 substantial source of aerosol. These relationships corroborate the ice nucleation observations, as discussed in detail below.

### 227 3.2 Variability in INP spectral properties based on storm characteristics

228 Out of the 25 aerosol, 30 rime, and 39 snow samples collected, 7 aerosol, 19 rime, and 23 snow were collected northwesterly or  
229 southeasterly case study days (Table 1). Mixed wind direction days were excluded, as sources from both directions would  
230 contribute to the daily aerosol sample. Figure 6 shows INP concentrations from aerosol, snow, and rime samples on the case days  
231 compared to air temperature, wind speed, and previous measurements at JFJ. Only the largest size range of the aerosol is shown  
232 because the remaining size ranges (i.e.,  $< 2.96 \mu\text{m}$ ) were not distinct with respect to wind direction. The fact that size, alone,  
233 exhibited directionally-dependent results and that such dependencies were only observed in the coarse mode aerosol indicate: (1)  
234 the sources were indeed different between northwesterly and southeasterly transport—supporting the air mass source analyses—  
235 and (2) the coarse mode aerosols were likely from a regional source as opposed to long-range transported thousands of kilometres.  
236 This is because gravitational settling typically renders transport of coarse particles inefficient especially within the boundary layer  
237 (Creamean et al., 2018a). Previous work by Collaud Coen et al. (2018) concludes that the local boundary layer never influences  
238 JFJ in the winter, supporting the fact that regional sources were likely prominent in the current work.

239 Generally, INPs from southeasterly days were higher in concentration and more efficient (i.e., were warm temperature INPs that  
240 facilitated ice formation  $> -15 \text{ }^\circ\text{C}$ ) than northwesterly samples. Our results are parallel to those by Stopelli et al. (2016), who also  
241 observed higher INP concentrations in snow samples collected during southerly conditions at JFJ from Dec 2012 to Oct 2014.  
242 However, when comparing overlapping temperature ranges from the snow samples during the winter only (Figure 6a),  
243 concentrations reported here are generally higher than those reported by Stopelli et al. (2016), especially at the highest  
244 temperatures. Aside from some of the snow samples, onset freezing temperatures (i.e., the highest temperature in which each  
245 sample froze) were higher for samples from the southeast as compared to the northwest (Figure 6b), indicating more efficient INPs  
246 from the southeast. However, a larger (smaller) spread in onset temperatures was observed in samples from the northwest  
247 (southeast), suggesting two possibilities: (1) influences were more (less) variable sources from the northwest (southeast), as  
248 discussed in more detail in the following section and/or (2) in the case of cloud rime and snow, clouds from the northwest were  
249 already depleted with the most efficient INPs due to precipitation prior to arriving at JFJ (i.e., higher transport altitudes which  
250 could have been exposed to cloudy conditions as compared to the southeast days which exhibited transport closer to the ground;  
251 Figures 3 and 4).

252 There was no clear correlation between INP concentrations with air temperature but air temperatures tended to be higher for  
253 northwesterly as compared to southeasterly cases. At  $-25 \text{ }^\circ\text{C}$  freezing temperatures for the INPs, most northwesterly samples had  
254 a range of INP concentrations at higher air temperatures (i.e.,  $> -9 \text{ }^\circ\text{C}$ ), while southeasterly samples exhibited overall higher INP  
255 concentrations, but still at a range of air temperatures (Figure 6e). In contrast, there was no correlation or gradient relationship  
256 between INP concentrations at any temperature and wind speed (Figure 6f – h), unlike the correlation between wind speed and  
257 INPs at  $-8 \text{ }^\circ\text{C}$  observed by Stopelli et al. (2016). We also evaluated INP concentrations versus wind speed at  $-8 \text{ }^\circ\text{C}$  but did not see  
258 any correlation (not shown). Regarding the snow, it is possible that surface processes generate airborne ice particles, which



259 contribute to a snow sample collected at a mountain station (Beck et al., 2018). However, snow that is re-suspended during a  
260 snowfall event largely consists of the most recently fallen snow crystals covering wind-exposed surfaces. These particles are  
261 unlikely to be different from concurrently falling snow. Hence, their contribution will not change INP abundance or spectral  
262 properties of the collected sample. Another matter are hoar frost crystals, which can be very abundant in terms of number, but  
263 because of their small size (i.e.,  $< 100 \mu\text{m}$  (Lloyd et al., 2015)) can only make a minor contribution to the mass of solid precipitation  
264 depositing in a tin placed horizontally on a mountain crest. The majority of small crystals will follow the streamlines of air passing  
265 over the crest. All that an increased influence of hoar frost particles would do to our observations is to decrease measured  
266 differences between snow and rime samples.

267 Figure 7 shows the cumulative and normalized differential INP spectra from the northwesterly and southeasterly case day samples.  
268 In addition to containing higher concentrations of warm temperature INPs, more southeasterly samples contained a bimodal  
269 distribution relative to the colder and unimodal distributions from northwesterly samples. The warm mode, or “bump” at  
270 temperatures above approximately  $-20 \text{ }^\circ\text{C}$  has been observed in a wide range of previous immersion mode ice nucleation studies  
271 including but not limited to some of the earliest studies of total aerosol (Vali, 1971), residuals found in hail (Vali and Stansbury,  
272 1966), sea spray aerosol (McCluskey et al., 2017; DeMott et al., 2016), soil samples (Hill et al., 2016), agricultural harvesting  
273 emissions (Suski et al., 2018), controlled laboratory measurements of mixtures of bacteria and illite (Beydoun et al., 2017), and in  
274 recent reviews of aerosol (Kanji et al., 2017; DeMott et al., 2018) and precipitation (Petters and Wright, 2015) samples. Most  
275 previous studies that show spectra with the warm mode typically: (1) report a wide range of freezing temperatures such that it can  
276 be observed relative to the steady increase of INPs at colder temperatures (i.e., Figure 7, left column) or (2) are of samples that  
277 include a mixture of biological and mineral or other less efficient INP sources. For example, several previous studies report INP  
278 concentrations down to only  $-15 \text{ }^\circ\text{C}$  (e.g., Conen and Yakutin, 2018; Hara et al., 2016; Kieft, 1988; Schnell and Vali, 1976; Vali  
279 et al., 1976; Wex et al., 2015), namely because the goal was to target efficient, warm-temperature biological INPs. However, the  
280 warm mode may not be evident in such studies, given it cannot be visualised next to the drastic increase in INPs with temperatures  
281 below  $-15 \text{ }^\circ\text{C}$  (i.e., the cold mode). In contrast, studies conducting INP measurements on known mineral dust samples also are not  
282 able to observe the warm mode (e.g., Price et al., 2018; Atkinson et al., 2013; Murray et al., 2012). Recent laboratory and modelling  
283 work by Beydoun et al. (2017) demonstrates the transition between warm and cold mode INPs using controlled experiments of  
284 Snowmax and illite mixtures. Together, it is apparent that a mixed biological and mineral (or less efficient biological INPs) sample  
285 is needed to assess the bimodal behaviour in the INP spectra.

### 286 3.3 Potential components of INP populations at JFJ

287 Taking the spectral characteristics in the context of air mass transport can help elucidate the possible sources of INPs at JFJ during  
288 INCAS. Qualitative and quantitative evaluation of the warm mode, or likely, the relative contribution of warm temperature  
289 biological INPs to cold mode INPs is transparent when differential INP spectra are calculated (Figure 7). Additionally, normalizing  
290 such spectra affords a qualitative comparison of spectra signatures between aerosols and residuals found in cloud rime and snow.

291 Figure 8 shows normalized differential spectral characteristics of daily aerosol, rime, and snow INPs. We offer some possible  
292 explanations for the observed variability between the samples. Naturally, the boundary layer more frequently than not contains  
293 higher concentrations of warm temperature INPs—and INPs in general—as compared to the free troposphere given the proximity  
294 to the sources (e.g., forests, agriculture, vegetation, and the oceans) (Burrows et al., 2013; Despres et al., 2012; Frohlich-Nowoisky  
295 et al., 2016; Wilson et al., 2015; Burrows et al., 2009a; Burrows et al., 2009b; Frohlich-Nowoisky et al., 2012; Suski et al., 2018).



296 Although, microorganisms and nanoscale biological fragments are episodically lofted into the free troposphere with mineral dust  
297 and transported thousands of kilometres (Creamean et al., 2013; Kellogg and Griffin, 2006).

298 Air arriving at JFJ on 15 and 16 Feb originated from the farthest away and were not heavily exposed to boundary layer air, as  
299 evidenced by the air mass trajectory analysis (Figure 3) and radon (Figure 5), indicating long-range transport in the free  
300 troposphere. This could explain why the warm mode was observed in the rime and snow, but not the aerosol—the aerosol had  
301 sufficient time to nucleate ice during free tropospheric transport and especially the warm temperature INPs that would likely  
302 become depleted in-cloud first (Stopelli et al., 2015), as also supported by the higher INP concentrations in most of the rime and  
303 snow compared to the aerosol in Figure 6b. Cloud fraction was relatively low (12.5 to 25%), but air temperatures were relatively  
304 high (−8.4 to −7.1 °C), suggesting conditions were amenable for long-range transported warm temperature INPs to nucleate cloud  
305 ice. However, from the available data, we cannot determine with certainty if the local conditions were the same as those when  
306 nucleation initially occurred. For 19 and 20 Feb, air temperature was very cold (−16.4 and −19.6 °C, respectively) cloud fraction  
307 was high (92 and 54%, respectively), and all samples remained unimodal (i.e., only containing the cold mode). One possible  
308 explanation is that any warm temperature INPs that were present in the clouds had already snowed out prior to reaching the  
309 sampling location, as observed by Stopelli et al. (2015) at JFJ. Although, given the low radon concentrations and erratic transport  
310 pathways, it is possible such air masses did not contain a relatively large concentrations of warm temperature INPs due to deficient  
311 exchange with the boundary layer. It was not until the southeasterly cases that the aerosol samples exhibited bimodal characteristics  
312 (i.e., contained both the warm and cold modes). Specifically, on 23 Feb local winds shifted to southeasterly (147 degrees on  
313 average) and air masses arrived from over the eastern Alps, Eastern Europe, Scandinavia, and earlier on in time, the Atlantic Ocean.  
314 Thus, these samples were predominantly influenced by the continental (mostly over remote regions) and marine boundary layers  
315 (Figures 4 and 5), where sources of warm temperature INPs are more abundant (Frohlich-Nowoisky et al., 2016). The northwesterly  
316 case of 06 Mar is somewhat interesting in that the local wind direction was clearly from the northwest, but air mass source analyses  
317 show transport in the boundary layer (radon) from the south, when looking farther back in time, traveling over the Mediterranean  
318 and North Africa. The aerosol sample had the third highest onset temperature for INPs (Figure 6b) and snow samples exhibited  
319 bimodality (Figure 8c). It is the only one of the northwesterly case samples that encountered boundary layer exposure according  
320 to the radon observations. Combined, these results suggest a somewhat mixed-source sample, and that 06 Mar may not be directly  
321 parallel to the other northwesterly cases. Transitioning back to a southeasterly case on 11 Mar, only the rime and snow unveiled  
322 bimodal behaviour from air transported from similar regions as the 06 Mar sample. However, transport on 11 Mar was more  
323 directly from the south over the Mediterranean and North Africa, indicating less time for removal of the INPs during transport.  
324 Additionally, OPC concentrations were very low (Figure 5). These results suggest the aerosols already nucleated cloud ice prior  
325 to reaching JFJ, which is supported by the 10 Mar sampling where the aerosol was bimodal, rime was unimodal, and snow was  
326 bimodal, but the warm mode resided at a relatively cold temperature (−16.5 °C).

327 Two other days without snowfall support the conclusion that southeasterly air mass transport introduces warm temperature INPs  
328 to JFJ. On 24 Feb, clouds were present at JFJ (a cloud fraction of 37.5%), but riming was insufficient to collect a sufficient quantity  
329 for INP analysis and no snowfall occurred. Interestingly, the warm mode was the maximum for the aerosol sample—normally, the  
330 cold mode has the highest normalized value—indicating a larger contribution of warm temperature INPs as compared to the total  
331 INP population. Air mass transport was very similar to 23 Feb signifying similar INP sources, but it is probable that a slightly  
332 warmer (−6.0 as compared to −9.8 °C air temperature), drier (79 versus 89% relative humidity), and higher pressure (649 versus  
333 645 mb) postfrontal system moved over JFJ on 24 Feb, inhibiting removal of warm temperature INPs during transport relative to  
334 the day prior. The second case, 28 Feb (not shown) was very similar to 24 Feb in that: (1) only an aerosol sample was collected



335 and (2) the warm mode was the maximum mode. As compared to 27 Feb where a warm mode was not observed, 28 Feb was  
336 warmer ( $-20.0$  as compared to  $-26.2$  °C), drier (52 versus 62%), higher pressure (635 versus 630 mb), and had a warmer onset  
337 temperature ( $-6.8$  versus  $-14.8$  °C). Wind direction was slightly different: southeasterly (153 degrees) on 27 Feb as compared to  
338 southwesterly on 28 Feb (221 degrees). However, conditions were cloudier than the 23 – 24 Feb coupling and completely cloudy  
339 on 27 Feb (100 and 66.7% cloud fraction on 27 Feb and 28 Feb, respectively). Additionally, radon and OPC concentrations were  
340 the highest on 27 – 28 Feb as compared to the rest of the days during INCAS (Figure 5). Combined, these results suggest a very  
341 local, boundary layer source of INPs started on 27 Feb, but were quickly depleted in the very cloudy conditions. Once clouds  
342 started to clear and a shift in frontal characteristics occurred, a similar source of very efficient warm temperature INPs affected JFJ  
343 but were able to be observed in the aerosol.

#### 344 4 Conclusions

345 Aerosol, cloud rime, and snow samples were collected at the High Altitude Research Station Jungfrauoch during the INCAS field  
346 campaign in Feb and Mar 2018. The objectives of the study were to assess variability in wintertime INP sources found in cloudy  
347 environments and evaluate relationships between INPs found in the different sample materials. To directly compare air to liquid  
348 samples, characteristics of normalized differential INP spectra were compared in the context of cumulative INP spectra statistics,  
349 air mass transport and exposure to boundary layer or free tropospheric conditions, and local meteorology. Distinction between  
350 northwesterly and southeasterly conditions yielded variable results regarding INP efficiency and concentrations, biological versus  
351 non-biological sources, and meteorological conditions at the sampling location. In general, INP concentrations were 3 to 20 times  
352 higher for all sample types when sources from the southeast infiltrated JFJ, while the modality of the INP spectra was bimodal for  
353 aerosol but variable for the rime and snow depending on meteorological context.

354 In general, comprehensive measurements of INPs from aerosol, and rime and snow when possible, affords useful information to  
355 compare and explain exchange between aerosols, clouds, and precipitation in the context of local and regional scale meteorology  
356 and transport conditions. Assessment of INP modality and spectra statistics adds another dimension for qualitative and semi-  
357 quantitative intercomparison of sampling days and evaluation of associations between aerosol, cloud, and precipitation sampling.  
358 Extending INP analyses past reporting cumulative concentrations affords more detailed information on the population of INPs and  
359 enables comparison between samples from aerosols, clouds, precipitation, and beyond (e.g., seawater, soil, etc.). Using auxiliary  
360 measurements and air mass simulations, in addition to context provided by previous work at JFJ, we have addressed possible  
361 sources for INCAS. However, more detailed source apportionment work should be imminent to comprehensively characterize INP  
362 sources based on spectral features. Future studies should ideally use such statistical analyses in tandem with focused chemical and  
363 biological characterization assessments to provide direct linkages between INP spectral properties and sources. Such investigations  
364 could yield valuable information on INP sources, and aerosol-cloud-precipitation interactions, which could then be used to improve  
365 process-level model parameterizations of such interactions by rendering quantitative information on INP source, efficiency, and  
366 abundance. Improving understanding of aerosol impacts on clouds and precipitation will ultimately significantly enhance  
367 understanding of the earth system with respect to cloud effects on the surface energy and water budgets to address future concerns  
368 of climate change and water availability.

#### 369 Author contributions



370 JMC collected the samples, conducted the DFA sample analysis, conducted data analysis, and wrote the manuscript. CM and FC  
371 also contributed to collecting rime and snow samples. JMC, CM, and FC designed the experiments. NB provided quality controlled  
372 OPS data. CM, NB, and FC helped with manuscript feedback and revision prior to submission.

### 373 Acknowledgements

374 The Swiss National Science Foundation (SNF) financially supported JMC within its Scientific Exchanges Programme, through  
375 grant number IZSEZ0\_179151. The work of CM and FC on Jungfraujoch is made possible through SNF grant number  
376 200021\_169620. Aerosol data were acquired by Paul Scherrer Institute in the framework of the Global Atmosphere Watch (GAW)  
377 programme funded by MeteoSwiss. Further support was received from the ACTRIS2 project funded through the EU H2020-  
378 INFRAIA-2014-2015 programme (grant agreement no. 654109) and the Swiss State Secretariat for Education, Research and  
379 Innovation (SERI; contract number 15.0159-1). The opinions expressed and arguments employed herein do not necessarily reflect  
380 the official views of the Swiss Government. We are grateful to the International Foundation High Altitude Research Stations  
381 Jungfraujoch and Gornergrat (HFSJG), 3012 Bern, Switzerland, for providing through its infrastructure comfortable access to  
382 mixed-phase clouds. Special thanks for go to Joan and Martin Fischer, and Christine and Ruedi Käser, the custodians of the station.  
383 The authors gratefully acknowledge the NOAA Air Resources Laboratory (ARL) for the provision of the HYSPLIT transport and  
384 dispersion model and/or READY website (<http://www.ready.noaa.gov>) used in this publication.

### 385 References

- 386 Albrecht, B. A.: Aerosols, Cloud Microphysics, and Fractional Cloudiness, *Science*, 245, 1227-1230,  
387 10.1126/science.245.4923.1227, 1989.
- 388 Alpert, P. A., Aller, J. Y., and Knopf, D. A.: Ice nucleation from aqueous NaCl droplets with and without marine diatoms, *Atmos.*  
389 *Chem. Phys.*, 11, 5539-5555, 10.5194/acp-11-5539-2011, 2011.
- 390 Atkinson, J. D., Murray, B. J., Woodhouse, M. T., Whale, T. F., Baustian, K. J., Carslaw, K. S., Dobbie, S., O'Sullivan, D., and  
391 Malkin, T. L.: The importance of feldspar for ice nucleation by mineral dust in mixed-phase clouds, *Nature*, 498, 355-  
392 358, 10.1038/nature12278, 2013.
- 393 Baltensperger, U., Gäggeler, H. W., Jost, D. T., Lugauer, M., Schwikowski, M., Weingartner, E., and Seibert, P.: Aerosol  
394 climatology at the high-alpine site Jungfraujoch, Switzerland, *Journal of Geophysical Research: Atmospheres*, 102,  
395 19707-19715, doi:10.1029/97JD00928, 1997.
- 396 Beck, A., Henneberger, J., Fugal, J. P., David, R. O., Lacher, L., and Lohmann, U.: Impact of surface and near-surface processes  
397 on ice crystal concentrations measured at mountain-top research stations, *Atmos Chem Phys*, 18, 8909-8927, 10.5194/acp-  
398 18-8909-2018, 2018.
- 399 Bergeron, T.: On the physics of cloud and precipitation, 5th Assembly of the U.G.G.I., Paul Dupont, Paris, 1935.
- 400 Beydoun, H., Polen, M., and Sullivan, R. C.: A new multicomponent heterogeneous ice nucleation model and its application to  
401 Snomax bacterial particles and a Snomax-illite mineral particle mixture, *Atmos Chem Phys*, 17, 13545-13557,  
402 10.5194/acp-17-13545-2017, 2017.
- 403 Bigg, E. K.: The Supercooling of Water, *P Phys Soc Lond B*, 66, 688-694, Doi 10.1088/0370-1301/66/8/309, 1953.
- 404 Boose, Y., Sierau, B., Garcia, M. I., Rodriguez, S., Alastuey, A., Linke, C., Schnaiter, M., Kupiszewski, P., Kanji, Z. A., and  
405 Lohmann, U.: Ice nucleating particles in the Saharan Air Layer, *Atmos. Chem. Phys.*, 16, 9067-9087, 2016.
- 406 Boucher, O., Randall, D., Artaxo, P., Bretherton, C., Feingold, G., Forster, P., Kerminen, V.-M., Kondo, Y., Liao, H., Lohmann,  
407 U., Rasch, P., Satheesh, S. K., Sherwood, S., Stevens, B., and Zhang, X. Y.: Clouds and Aerosols, in: *Climate Change*  
408 *2013: The Physical Science Basis. Contribution of Working Group I to the Fifth Assessment Report of the*  
409 *Intergovernmental Panel on Climate Change*, edited by: Stocker, T. F., Qin, D., Plattner, G.-K., Tignor, M., Allen, S. K.,  
410 Boschung, J., Nauels, A., Xia, Y., Bex, V., and Midgley, P. M., Cambridge University Press, Cambridge, United Kingdom  
411 and New York, NY, USA, 571-658, 2013.
- 412 Bowers, R. M., Lauber, C. L., Wiedinmyer, C., Hamady, M., Hallar, A. G., Fall, R., Knight, R., and Fierer, N.: Characterization  
413 of Airborne Microbial Communities at a High-Elevation Site and Their Potential To Act as Atmospheric Ice Nuclei, *Appl*  
414 *Environ Microb*, 75, 5121-5130, 10.1128/Aem.00447-09, 2009.
- 415 Bukowiecki, N., Weingartner, E., Gysel, M., Coen, M. C., Zieger, P., Herrmann, E., Steinbacher, M., Gäggeler, H. W., and  
416 Baltensperger, U.: A Review of More than 20 Years of Aerosol Observation at the High Altitude Research Station  
417 Jungfraujoch, Switzerland (3580 m asl), *Aerosol Air Qual Res*, 16, 764-788, 10.4209/aaqr.2015.05.0305, 2016.



- 418 Burrows, S. M., Butler, T., Jockel, P., Tost, H., Kerkweg, A., Poschl, U., and Lawrence, M. G.: Bacteria in the global atmosphere  
419 - Part 2: Modeling of emissions and transport between different ecosystems, *Atmos Chem Phys*, 9, 9281-9297, DOI  
420 10.5194/acp-9-9281-2009, 2009a.
- 421 Burrows, S. M., Elbert, W., Lawrence, M. G., and Poschl, U.: Bacteria in the global atmosphere - Part 1: Review and synthesis of  
422 literature data for different ecosystems, *Atmos Chem Phys*, 9, 9263-9280, DOI 10.5194/acp-9-9263-2009, 2009b.
- 423 Burrows, S. M., Hoose, C., Poschl, U., and Lawrence, M. G.: Ice nuclei in marine air: biogenic particles or dust?, *Atmos Chem*  
424 *Phys*, 13, 245-267, 10.5194/acp-13-245-2013, 2013.
- 425 Chambers, S. D., Williams, A. G., Conen, F., Griffiths, A. D., Reimann, S., Steinbacher, M., Krummel, P. B., Steele, L. P., van  
426 der Schoot, M. V., Galbally, I. E., Molloy, S. B., and Barnes, J. E.: Towards a Universal "Baseline" Characterisation of  
427 Air Masses for High- and Low-Altitude Observing Stations Using Radon-222, *Aerosol Air Qual Res*, 16, 885-899,  
428 10.4209/aaqr.2015.06.0391, 2016.
- 429 Christner, B. C., Morris, C. E., Foreman, C. M., Cai, R. M., and Sands, D. C.: Ubiquity of biological ice nucleators in snowfall,  
430 *Science*, 319, 1214-1214, 10.1126/science.1149757, 2008.
- 431 Collaud Coen, M., Weingartner, E., Schaub, D., Hueglin, C., Corrigan, C., Henning, S., Schwikowski, M., and Baltensperger, U.:  
432 Saharan dust events at the Jungfraujoch: detection by wavelength dependence of the single scattering albedo and first  
433 climatology analysis, *Atmos. Chem. Phys.*, 4, 2465-2480, 2004.
- 434 Collaud Coen, M., Andrews, E., Aliaga, D., Andrade, M., Angelov, H., Bukowiecki, N., Ealo, M., Fialho, P., Flentje, H., Hallar,  
435 A. G., Hooda, R., Kalapov, I., Krejci, R., Lin, N.-H., Marinoni, A., Ming, J., Nguyen, N. A., Pandolfi, M., Pont, V., Ries,  
436 L., Rodriguez, S., Schauer, G., Sellegri, K., Sharma, S., Sun, J., Tunved, P., Velasquez, P., and Ruffieux, D.: Identification  
437 of topographic features influencing aerosol observations at high altitude stations, *Atmos. Chem. Phys.*, 18, 12289-12313,  
438 2018.
- 439 Coluzza, I., Creamean, J., Rossi, M., Wex, H., Alpert, P., Bianco, V., Boose, Y., Dellago, C., Felgitsch, L., Fröhlich-Nowoisky,  
440 J., Herrmann, H., Jungblut, S., Kanji, Z., Menzl, G., Moffett, B., Moritz, C., Mutzel, A., Pöschl, U., Schauer, M., Scheel,  
441 J., Stopelli, E., Stratmann, F., Grothe, H., and Schmale, D.: Perspectives on the Future of Ice Nucleation Research:  
442 Research Needs and Unanswered Questions Identified from Two International Workshops, *Atmosphere*, 8, 138, 2017.
- 443 Conen, F., Morris, C. E., Leifeld, J., Yakutin, M. V., and Alewell, C.: Biological residues define the ice nucleation properties of  
444 soil dust, *Atmos. Chem. Phys.*, 11, 9643-9648, 10.5194/acp-11-9643-2011, 2011.
- 445 Conen, F., Rodriguez, S., Huglin, C., Henne, S., Herrmann, E., Bukowiecki, N., and Alewell, C.: Atmospheric ice nuclei at the  
446 high-altitude observatory Jungfraujoch, Switzerland, *Tellus B*, 67, 10.3402/tellusb.v67.25014, 2015.
- 447 Conen, F., and Yakutin, M. V.: Soils rich in biological ice-nucleating particles abound in ice-nucleating macromolecules likely  
448 produced by fungi, *Biogeosciences*, 15, 4381-4385, 10.5194/bg-15-4381-2018, 2018.
- 449 Creamean, J. M., Suski, K. J., Rosenfeld, D., Cazorla, A., DeMott, P. J., Sullivan, R. C., White, A. B., Ralph, F. M., Minnis, P.,  
450 Comstock, J. M., Tomlinson, J. M., and Prather, K. A.: Dust and Biological Aerosols from the Sahara and Asia Influence  
451 Precipitation in the Western U.S., *Science*, 339, 1572-1578, DOI 10.1126/science.1227279, 2013.
- 452 Creamean, J. M., Kirpes, R. M., Pratt, K. A., Spada, N. S., Maahn, M., de Boer, G., Schnell, R. C., and China, S.: Marine and  
453 terrestrial influences on ice nucleating particles during continuous springtime measurements in an Arctic oilfield location,  
454 *Atmos Chem Phys*, in preparation, 2018a.
- 455 Creamean, J. M., Primm, K. M., Tolbert, M. A., Hall, E. G., Wendell, J., Jordan, A., Sheridan, P. J., Smith, J., and Schnell, R. C.:  
456 HOVERCAT: A novel aerial system for evaluation of aerosol-cloud interactions, *Atmos. Meas. Tech.*, submitted, 2018b.
- 457 Cziczo, D. J., Ladino, L., Boose, Y., Kanji, Z. A., Kupiszewski, P., Lance, S., Mertes, S., and Wex, H.: Measurements of Ice  
458 Nucleating Particles and Ice Residuals, *Meteorological Monographs*, 58, 8.1-8.13, 10.1175/amsmonographs-d-16-0008.1,  
459 2017.
- 460 DeMott, P. J., Chen, Y., Kreidenweis, S. M., Rogers, D. C., and Sherman, D. E.: Ice formation by black carbon particles, *Geophys*  
461 *Res Lett*, 26, 2429-2432, Doi 10.1029/1999gl900580, 1999.
- 462 DeMott, P. J., Prenni, A. J., Liu, X., Kreidenweis, S. M., Petters, M. D., Twohy, C. H., Richardson, M. S., Eidhammer, T., and  
463 Rogers, D. C.: Predicting global atmospheric ice nuclei distributions and their impacts on climate, *P Natl Acad Sci USA*,  
464 107, 11217-11222, 10.1073/pnas.0910818107, 2010.
- 465 DeMott, P. J., Hill, T. C. J., McCluskey, C. S., Prather, K. A., Collins, D. B., Sullivan, R. C., Ruppel, M. J., Mason, R. H., Irish,  
466 V. E., Lee, T., Hwang, C. Y., Rhee, T. S., Snider, J. R., McMeeking, G. R., Dhaniyala, S., Lewis, E. R., Wentzell, J. J.  
467 B., Abbatt, J., Lee, C., Sultana, C. M., Ault, A. P., Axson, J. L., Martinez, M. D., Venero, I., Santos-Figueroa, G., Stokes,  
468 M. D., Deane, G. B., Mayol-Bracero, O. L., Grassian, V. H., Bertram, T. H., Bertram, A. K., Moffett, B. F., and Franc,  
469 G. D.: Sea spray aerosol as a unique source of ice nucleating particles, *P Natl Acad Sci USA*, 113, 5797-5803,  
470 10.1073/pnas.1514034112, 2016.
- 471 DeMott, P. J., Möhler, O., Cziczo, D. J., Hiranuma, N., Petters, M. D., Petters, S. S., Belosi, F., Bingemer, H. G., Brooks, S. D.,  
472 Budke, C., Burkert-Kohn, M., Collier, K. N., Danielczok, A., Eppers, O., Felgitsch, L., Garimella, S., Grothe, H., Herenz,  
473 P., Hill, T. C. J., Höhler, K., Kanji, Z. A., Kiselev, A., Koop, T., Kristensen, T. B., Krüger, K., Kulkarni, G., Levin, E. J.  
474 T., Murray, B. J., Nicosia, A. D., O. S., A., P., J., P. M., C., P. H., Reicher, N., Rothenberg, D. A., Rudich, Y., Santachiara,  
475 G., Schiebel, T., Schrod, J., Seifried, T. M., Stratmann, F., Sullivan, R. C., Suski, K. J., Szakáll, M., Taylor, H. P., Ullrich,  
476 R., Vergara-Temprado, J., Wagner, R., Whale, T. F., Weber, D., Welti, A., Wilson, T. W., Wolf, M. J., and Zenker, J.:



- 477 The Fifth International Workshop on Ice Nucleation phase 2 (FIN-02): Laboratory intercomparison of ice nucleation  
478 measurements, *Atmos. Meas. Tech.*, in review, <https://doi.org/10.5194/amt-2018-191>, 2018.
- 479 Despres, V. R., Huffman, J. A., Burrows, S. M., Hoose, C., Safatov, A. S., Buryak, G., Frohlich-Nowoisky, J., Elbert, W., Andreae,  
480 M. O., Poschl, U., and Jaenicke, R.: Primary biological aerosol particles in the atmosphere: a review, *Tellus B*, 64,  
481 10.3402/tellusb.v64i0.15598, 2012.
- 482 Draxler, R. R.: HYSPLIT4 user's guide, NOAA Air Resources Laboratory, Silver Spring, MD., 1999.
- 483 Draxler, R. R., and Rolph, G.: HYSPLIT (HYbrid Single-Particle Lagrangian Integrated Trajectory) Model access via NOAA ARL  
484 READY website (<http://ready.arl.noaa.gov/hysplit.php>), NOAA Air Resources Laboratory, Silver Spring, MD, 2011.
- 485 Eriksen Hammer, S., Mertes, S., Schneider, J., Ebert, M., Kandler, K., and Weinbruch, S.: Composition of ice particle residuals in  
486 mixed-phase clouds at Jungfrauoch (Switzerland): enrichment and depletion of particle groups relative to total aerosol,  
487 *Atmos. Chem. Phys.*, 18, 13987-14003, 2018.
- 488 Fridlind, A. M., Diedenhoven, B. v., Ackerman, A. S., Avramov, A., Mrowiec, A., Morrison, H., Zuidema, P., and Shupe, M. D.:  
489 A FIRE-ACE/SHEBA Case Study of Mixed-Phase Arctic Boundary Layer Clouds: Entrainment Rate Limitations on  
490 Rapid Primary Ice Nucleation Processes, *Journal of the Atmospheric Sciences*, 69, 365-389, 10.1175/jas-d-11-052.1,  
491 2012.
- 492 Frohlich-Nowoisky, J., Burrows, S. M., Xie, Z., Engling, G., Solomon, P. A., Fraser, M. P., Mayol-Bracero, O. L., Artaxo, P.,  
493 Begerow, D., Conrad, R., Andreae, M. O., Despres, V. R., and Poschl, U.: Biogeography in the air: fungal diversity over  
494 land and oceans, *Biogeosciences*, 9, 1125-1136, 10.5194/bg-9-1125-2012, 2012.
- 495 Frohlich-Nowoisky, J., Kampf, C. J., Weber, B., Huffman, J. A., Pohlker, C., Andreae, M. O., Lang-Yona, N., Burrows, S. M.,  
496 Gunthe, S. S., Elbert, W., Su, H., Hoor, P., Thines, E., Hoffmann, T., Despres, V. R., and Poschl, U.: Bioaerosols in the  
497 Earth system: Climate, health, and ecosystem interactions, *Atmos Res*, 182, 346-376, 10.1016/j.atmosres.2016.07.018,  
498 2016.
- 499 Fröhlich-Nowoisky, J., Hill, T. C. J., Pummer, B. G., Yordanova, P., Franc, G. D., and Pöschl, U.: Ice nucleation activity in the  
500 widespread soil fungus *Mortierella alpina*, *Biogeosciences*, 12, 1057-1071, 10.5194/bg-12-1057-2015, 2015.
- 501 Ganguly, M., Dib, S., and Ariya, P. A.: Purely Inorganic Highly Efficient Ice Nucleating Particle, *ACS Omega*, 3, 3384-3395,  
502 10.1021/acsomega.7b01830, 2018.
- 503 Griffiths, A. D., Conen, F., Weingartner, E., Zimmermann, L., Chambers, S. D., Williams, A. G., and Steinbacher, M.: Surface-  
504 to-mountaintop transport characterised by radon observations at the Jungfrauoch, *Atmos Chem Phys*, 14, 12763-12779,  
505 10.5194/acp-14-12763-2014, 2014.
- 506 Hader, J. D., Wright, T. P., and Petters, M. D.: Contribution of pollen to atmospheric ice nuclei concentrations, *Atmos. Chem.*  
507 *Phys.*, 14, 5433-5449, 10.5194/acp-14-5433-2014, 2014a.
- 508 Hader, J. D., Wright, T. P., and Petters, M. D.: Contribution of pollen to atmospheric ice nuclei concentrations, *Atmos Chem Phys*,  
509 14, 5433-5449, 10.5194/acp-14-5433-2014, 2014b.
- 510 Hara, K., Maki, T., Kakikawa, M., Kobayashi, F., and Matsuki, A.: Effects of different temperature treatments on biological ice  
511 nuclei in snow samples, *Atmos Environ*, 140, 415-419, 10.1016/j.atmosenv.2016.06.011, 2016.
- 512 Herrmann, E., Weingartner, E., Henne, S., Vuilleumier, L., Bukowiecki, N., Steinbacher, M., Conen, F., Coen, M. C., Hammer,  
513 E., Juranyi, Z., Baltensperger, U., and Gysel, M.: Analysis of long-term aerosol size distribution data from Jungfrauoch  
514 with emphasis on free tropospheric conditions, cloud influence, and air mass transport, *J Geophys Res-Atmos*, 120, 9459-  
515 9480, 10.1002/2015jd023660, 2015.
- 516 Hill, T. C. J., DeMott, P. J., Tobo, Y., Fröhlich-Nowoisky, J., Moffett, B. F., Franc, G. D., and Kreidenweis, S. M.: Sources of  
517 organic ice nucleating particles in soils, *Atmos. Chem. Phys.*, 16, 7195-7211, 10.5194/acp-16-7195-2016, 2016.
- 518 Hoose, C., and Möhler, O.: Heterogeneous ice nucleation on atmospheric aerosols: a review of results from laboratory experiments,  
519 *Atmos. Chem. Phys.*, 12, 9817-9854, 10.5194/acp-12-9817-2012, 2012.
- 520 Hu, W., Niu, H. Y., Murata, K., Wu, Z. J., Hu, M., Kojima, T., and Zhang, D. Z.: Bacteria in atmospheric waters: Detection,  
521 characteristics and implications, *Atmos Environ*, 179, 201-221, 10.1016/j.atmosenv.2018.02.026, 2018.
- 522 Hummel, M., Hoose, C., Gallagher, M., Healy, D. A., Huffman, J. A., O'Connor, D., Poschl, U., Pohlker, C., Robinson, N. H.,  
523 Schnaiter, M., Sodeau, J. R., Stengel, M., Toprak, E., and Vogel, H.: Regional-scale simulations of fungal spore aerosols  
524 using an emission parameterization adapted to local measurements of fluorescent biological aerosol particles, *Atmos*  
525 *Chem Phys*, 15, 6127-6146, 10.5194/acp-15-6127-2015, 2015.
- 526 Jaenicke, R.: Abundance of Cellular Material and Proteins in the Atmosphere, *Science*, 308, 73-73, 10.1126/science.1106335,  
527 2005.
- 528 Jaenicke, R., Matthias-Maser, S., and Gruber, S.: Omnipresence of biological material in the atmosphere, *Environmental*  
529 *Chemistry*, 4, 217-220, <https://doi.org/10.1071/EN07021>, 2007.
- 530 Kanji, Z. A., Ladino, L. A., Wex, H., Boose, Y., Burkert-Kohn, M., Cziczo, D. J., and Krämer, M.: Overview of Ice Nucleating  
531 Particles, *Meteorological Monographs*, 58, 1.1-1.33, 10.1175/amsmonographs-d-16-0006.1, 2017.
- 532 Kellogg, C. A., and Griffin, D. W.: Aerobiology and the global transport of desert dust, *Trends Ecol Evol*, 21, 638-644,  
533 10.1016/j.tree.2006.07.004, 2006.
- 534 Kieft, T. L.: Ice Nucleation Activity in Lichens, *Appl Environ Microb*, 54, 1678-1681, 1988.
- 535 Knopf, D. A., Alpert, P. A., Wang, B., and Aller, J. Y.: Stimulation of ice nucleation by marine diatoms, *Nature Geoscience*, 4,  
536 88, 10.1038/ngeo1037, 2010.



- 537 Korolev, A., McFarquhar, G., Field, P. R., Franklin, C., Lawson, P., Wang, Z., Williams, E., Abel, S. J., Axisa, D., Borrmann, S.,  
538 Crosier, J., Fugal, J., Krämer, M., Lohmann, U., Schlenker, O., Schnaiter, M., and Wendisch, M.: Mixed-Phase Clouds:  
539 Progress and Challenges, *Meteorological Monographs*, 58, 5.1-5.50, [10.1175/amsmonographs-d-17-0001.1](https://doi.org/10.1175/amsmonographs-d-17-0001.1), 2017.
- 540 Lacher, L., Lohmann, U., Boose, Y., Zipori, A., Herrmann, E., Bukowiecki, N., Steinbacher, M., and Kanji, Z. A.: The Horizontal  
541 Ice Nucleation Chamber (HINC): INP measurements at conditions relevant for mixed-phase clouds at the High Altitude  
542 Research Station Jungfraujoch, *Atmos. Chem. Phys.*, 17, 15199–15224, <https://doi.org/10.5194/acp-17-15199-2017>,  
543 2017.
- 544 Lacher, L., DeMott, P. J., Levin, E. J. T., Suski, K. J., Boose, Y., Zipori, A., Herrmann, E., Bukowiecki, N., Steinbacher, M., Gute,  
545 E., Abbatt, J. P. D., Lohmann, U., and Kanji, Z. A.: Background Free-Tropospheric Ice Nucleating Particle Concentrations  
546 at Mixed-Phase Cloud Conditions, *Journal of Geophysical Research: Atmospheres*, 123, doi:10.1029/2018JD028338,  
547 2018a.
- 548 Lacher, L., Steinbacher, M., Bukowiecki, N., Herrmann, E., Zipori, A., and Kanji, Z. A.: Impact of Air Mass Conditions and  
549 Aerosol Properties on Ice Nucleating Particle Concentrations at the High Altitude Research Station Jungfraujoch,  
550 *Atmosphere*, 9, 2018b.
- 551 Langham, E. J., and Mason, B. J.: The Heterogeneous and Homogeneous Nucleation of Supercooled Water, *Proc R Soc Lon Ser-*  
552 *A*, 247, 493-&, DOI 10.1098/rspa.1958.0207, 1958.
- 553 Lloyd, G., Chouarton, T. W., Bower, K. N., Gallagher, M. W., Connolly, P. J., Flynn, M., Farrington, R., Crosier, J., Schlenker,  
554 O., Fugal, J., and Henneberger, J.: The origins of ice crystals measured in mixed-phase clouds at the high-alpine site  
555 Jungfraujoch, *Atmos Chem Phys*, 15, 12953-12969, [10.5194/acp-15-12953-2015](https://doi.org/10.5194/acp-15-12953-2015), 2015.
- 556 Lohmann, U., Henneberger, J., Henneberg, O., Fugal, J. P., Bühl, J., and Kanji, Z. A.: Persistence of orographic mixed-phase  
557 clouds, *Geophys Res Lett*, 43, 10,512-510,519, doi:10.1002/2016GL071036, 2016.
- 558 Mason, R. H., Si, M., Chou, C., Irish, V. E., Dickie, R., Elizondo, P., Wong, R., Brintnell, M., Elsasser, M., Lassar, W. M., Pierce,  
559 K. M., Leaitch, W. R., MacDonald, A. M., Platt, A., Toom-Sauntry, D., Sarda-Esteve, R., Schiller, C. L., Suski, K. J.,  
560 Hill, T. C. J., Abbatt, J. P. D., Huffman, J. A., DeMott, P. J., and Bertram, A. K.: Size-resolved measurements of ice-  
561 nucleating particles at six locations in North America and one in Europe, *Atmos Chem Phys*, 16, 1637-1651, [10.5194/acp-](https://doi.org/10.5194/acp-16-1637-2016)  
562 [16-1637-2016](https://doi.org/10.5194/acp-16-1637-2016), 2016.
- 563 McCluskey, C. S., Hill, T. C. J., Malfatti, F., Sultana, C. M., Lee, C., Santander, M. V., Beall, C. M., Moore, K. A., Cornwell, G.  
564 C., Collins, D. B., Prather, K. A., Jayarathne, T., Stone, E. A., Azam, F., Kreidenweis, S. M., and DeMott, P. J.: A  
565 Dynamic Link between Ice Nucleating Particles Released in Nascent Sea Spray Aerosol and Oceanic Biological Activity  
566 during Two Mesocosm Experiments, *Journal of the Atmospheric Sciences*, 74, 151-166, [10.1175/Jas-D-16-0087.1](https://doi.org/10.1175/Jas-D-16-0087.1), 2017.
- 567 Mignani, C., Creamean, J. M., Zimmermann, L., Alewell, C., and Conen, F.: Direct evidence for secondary ice formation at around  
568 -15 °C in mixed-phase clouds, *Atmos. Chem. Phys. Discuss.*, under review, 2018.
- 569 Morris, C. E., Georgakopoulos, D. G., and Sands, D. C.: Ice nucleation active bacteria and their potential role in precipitation, *J*  
570 *Phys Iv*, 121, 87-103, DOI 10.1051/jp4:2004121004, 2004.
- 571 Morris, C. E., Sands, D. C., Bardin, M., Jaenicke, R., Vogel, B., Leyronas, C., Ariya, P. A., and Psenner, R.: Microbiology and  
572 atmospheric processes: research challenges concerning the impact of airborne micro-organisms on the atmosphere and  
573 climate, *Biogeosciences*, 8, 17-25, [10.5194/bg-8-17-2011](https://doi.org/10.5194/bg-8-17-2011), 2011.
- 574 Morris, C. E., Conen, F., Huffman, J. A., Phillips, V., Poschl, U., and Sands, D. C.: Bioprecipitation: a feedback cycle linking  
575 Earth history, ecosystem dynamics and land use through biological ice nucleators in the atmosphere, *Global Change Biol*,  
576 20, 341-351, [10.1111/gcb.12447](https://doi.org/10.1111/gcb.12447), 2014.
- 577 Morris, C. E., Soubeyrand, S., Bigg, E. K., Creamean, J. M., and Sands, D. C.: Mapping Rainfall Feedback to Reveal the Potential  
578 Sensitivity of Precipitation to Biological Aerosols, *Bulletin of the American Meteorological Society*, 98, 1109-1118,  
579 <https://doi.org/10.1175/BAMS-D-15-00293.1>, 2017.
- 580 Mossop, S. C., and Thorndike, N. S. C.: The Use of Membrane Filters in Measurements of Ice Nucleus Concentration. I. Effect of  
581 Sampled Air Volume, *Journal of Applied Meteorology*, 5, 474-480, [10.1175/1520-](https://doi.org/10.1175/1520-0450(1966)005<0474:tuomfi>2.0.co;2)  
582 [0450\(1966\)005<0474:tuomfi>2.0.co;2](https://doi.org/10.1175/1520-0450(1966)005<0474:tuomfi>2.0.co;2), 1966.
- 583 Murray, B. J., O'Sullivan, D., Atkinson, J. D., and Webb, M. E.: Ice nucleation by particles immersed in supercooled cloud droplets,  
584 *Chem Soc Rev*, 41, 6519-6554, Doi 10.1039/C2cs35200a, 2012.
- 585 O'Sullivan, D., Murray, B. J., Malkin, T. L., Whale, T. F., Umo, N. S., Atkinson, J. D., Price, H. C., Baustian, K. J., Browse, J.,  
586 and Webb, M. E.: Ice nucleation by fertile soil dusts: relative importance of mineral and biogenic components, *Atmos.*  
587 *Chem. Phys.*, 14, 1853-1867, [10.5194/acp-14-1853-2014](https://doi.org/10.5194/acp-14-1853-2014), 2014.
- 588 O'Sullivan, D., Murray, B. J., Ross, J. F., and Webb, M. E.: The adsorption of fungal ice-nucleating proteins on mineral dusts: a  
589 terrestrial reservoir of atmospheric ice-nucleating particles, *Atmos Chem Phys*, 16, 7879-7887, [10.5194/acp-16-7879-](https://doi.org/10.5194/acp-16-7879-2016)  
590 [2016](https://doi.org/10.5194/acp-16-7879-2016), 2016.
- 591 Petters, M. D., and Wright, T. P.: Revisiting ice nucleation from precipitation samples, *Geophys Res Lett*, 42, 8758-8766,  
592 [10.1002/2015gl065733](https://doi.org/10.1002/2015gl065733), 2015.
- 593 Polen, M., Brubaker, T., Somers, J., and Sullivan, R. C.: Cleaning up our water: reducing interferences from nonhomogeneous  
594 freezing of "pure" water in droplet freezing assays of ice-nucleating particles, *Atmos Meas Tech*, 11, 5315-5334,  
595 [10.5194/amt-11-5315-2018](https://doi.org/10.5194/amt-11-5315-2018), 2018.



- 596 Price, H. C., Baustian, K. J., McQuaid, J. B., Blyth, A., Bower, K. N., Choularton, T., Cotton, R. J., Cui, Z., Field, P. R., Gallagher,  
597 M., Hawker, R., Merrington, A., Miltenberger, A., Neely, R. R., Parker, S. T., Rosenberg, P. D., Taylor, J. W., Trembath,  
598 J., Vergara-Temprado, J., Whale, T. F., Wilson, T. W., Young, G., and Murray, B. J.: Atmospheric Ice-Nucleating  
599 Particles in the Dusty Tropical Atlantic, *J Geophys Res-Atmos*, 123, 2175-2193, 10.1002/2017jd027560, 2018.
- 600 Reche, I., D'Orta, G., Mladenov, N., Winget, D. M., and Suttle, C. A.: Deposition rates of viruses and bacteria above the  
601 atmospheric boundary layer, *Isme J*, 12, 1154-1162, 10.1038/s41396-017-0042-4, 2018.
- 602 Sahyoun, M., Korsholm, U. S., Sorensen, J. H., Santl-Temkiv, T., Finster, K., Gosewinkel, U., and Nielsen, N. W.: Impact of  
603 bacterial ice nucleating particles on weather predicted by a numerical weather prediction model, *Atmos Environ*, 170, 33-  
604 44, 10.1016/j.atmosenv.2017.09.029, 2017.
- 605 Schnell, R. C., and Vali, G.: Biogenic Ice Nuclei .1. Terrestrial and Marine Sources, *Journal of the Atmospheric Sciences*, 33,  
606 1554-1564, Doi 10.1175/1520-0469(1976)033<1554:Binpit>2.0.Co;2, 1976.
- 607 Stein, A. F., Draxler, R. R., Rolph, G. D., Stunder, B. J. B., Cohen, M. D., and Ngan, F.: NOAA's HYSPLIT Atmospheric Transport  
608 and Dispersion Modeling System, *Bulletin of the American Meteorological Society*, 96, 2059-2077, 10.1175/bams-d-14-  
609 00110.1, 2015.
- 610 Stopelli, E., Conen, F., Zimmermann, L., Alewell, C., and Morris, C. E.: Freezing nucleation apparatus puts new slant on study of  
611 biological ice nucleators in precipitation, *Atmos Meas Tech*, 7, 129-134, 10.5194/amt-7-129-2014, 2014.
- 612 Stopelli, E., Conen, F., Morris, C. E., Herrmann, E., Bukowiecki, N., and Alewell, C.: Ice nucleation active particles are efficiently  
613 removed by precipitating clouds, *Scientific Reports*, 5, 16433, 10.1038/srep16433, 2015.
- 614 Stopelli, E., Conen, F., Morris, C. E., Herrmann, E., Henne, S., Steinbacher, M., and Alewell, C.: Predicting abundance and  
615 variability of ice nucleating particles in precipitation at the high-altitude observatory Jungfraujoch, *Atmos Chem Phys*,  
616 16, 8341-8351, 10.5194/acp-16-8341-2016, 2016.
- 617 Stopelli, E., Conen, F., Guilbaud, C., Zopfi, J., Alewell, C., and Morris, C. E.: Ice nucleators, bacterial cells and *Pseudomonas*  
618 *syringae* in precipitation at Jungfraujoch, *Biogeosciences*, 14, 1189-1196, 10.5194/bg-14-1189-2017, 2017.
- 619 Storelvmo, T., Hoose, C., and Eriksson, P.: Global modeling of mixed-phase clouds: The albedo and lifetime effects of aerosols,  
620 *Journal of Geophysical Research: Atmospheres*, 116, doi:10.1029/2010JD014724, 2011.
- 621 Suski, K. J., Hill, T. C. J., Levin, E. J. T., Miller, A., DeMott, P. J., and Kreidenweis, S. M.: Agricultural harvesting emissions of  
622 ice-nucleating particles, *Atmos. Chem. Phys.*, 18, 13755-13771, 2018.
- 623 Tesson, S. V. M., Skj oth, C. A., Santl-Temkiv, T., and L ndahl, J.: Airborne Microalgae: Insights, Opportunities and Challenges,  
624 *Appl Environ Microb*, 10.1128/aem.03333-15, 2016.
- 625 Tobo, Y., DeMott, P. J., Hill, T. C. J., Prenni, A. J., Swoboda-Colberg, N. G., Franc, G. D., and Kreidenweis, S. M.: Organic matter  
626 matters for ice nuclei of agricultural soil origin, *Atmos. Chem. Phys.*, 14, 8521-8531, 10.5194/acp-14-8521-2014, 2014.
- 627 Tobo, Y.: An improved approach for measuring immersion freezing in large droplets over a wide temperature range, *Scientific*  
628 *Reports*, 6, ARTN 3293010.1038/srep32930, 2016.
- 629 Twohy, C. H., McMeeking, G. R., DeMott, P. J., McCluskey, C. S., Hill, T. C. J., Burrows, S. M., Kulkarni, G. R., Tanarhte, M.,  
630 Kafle, D. N., and Toohey, D. W.: Abundance of fluorescent biological aerosol particles at temperatures conducive to the  
631 formation of mixed-phase and cirrus clouds, *Atmos Chem Phys*, 16, 8205-8225, 10.5194/acp-16-8205-2016, 2016.
- 632 Twomey, S.: The Influence of Pollution on the Shortwave Albedo of Clouds, *Journal of the Atmospheric Sciences*, 34, 1149-1152,  
633 10.1175/1520-0469(1977)034<1149:tiopot>2.0.co;2, 1977.
- 634 Vali, G., and Stansbury, E. J.: Time-Dependent Characteristics of Heterogeneous Nucleation of Ice, *Can J Phys*, 44, 477-+, DOI  
635 10.1139/p66-044, 1966.
- 636 Vali, G.: Quantitative Evaluation of Experimental Results an the Heterogeneous Freezing Nucleation of Supercooled Liquids,  
637 *Journal of the Atmospheric Sciences*, 28, 402-409, 10.1175/1520-0469(1971)028<0402:qeora>2.0.co;2, 1971.
- 638 Vali, G., Christensen, M., Fresh, R. W., Galyan, E. L., Maki, L. R., and Schnell, R. C.: Biogenic Ice Nuclei .2. Bacterial Sources,  
639 *Journal of the Atmospheric Sciences*, 33, 1565-1570, Doi 10.1175/1520-0469(1976)033<1565:Binpib>2.0.Co;2, 1976.
- 640 von Blohn, N., Mitra, S. K., Diehl, K., and Borrmann, S.: The ice nucleating ability of pollen: Part III: New laboratory studies in  
641 immersion and contact freezing modes including more pollen types, *Atmos Res*, 78, 182-189,  
642 10.1016/j.atmosres.2005.03.008, 2005.
- 643 Weingartner, E., Nyeki, S., and Baltensperger, U.: Seasonal and diurnal variation of aerosol size distributions ( $10 < D < 750$  nm)  
644 at a high-alpine site (Jungfraujoch 3580 m asl), *J Geophys Res-Atmos*, 104, 26809-26820, Doi 10.1029/1999jd00170,  
645 1999.
- 646 Wex, H., Augustin-Bauditz, S., Boose, Y., Budke, C., Curtius, J., Diehl, K., Dreyer, A., Frank, F., Hartmann, S., Hiranuma, N.,  
647 Jantsch, E., Kanji, Z. A., Kiselev, A., Koop, T., Mohler, O., Niedermeier, D., Nillius, B., Rosch, M., Rose, D., Schmidt,  
648 C., Steinke, I., and Stratmann, F.: Intercomparing different devices for the investigation of ice nucleating particles using  
649 Snomax (R) as test substance, *Atmos Chem Phys*, 15, 1463-1485, 10.5194/acp-15-1463-2015, 2015.
- 650 Wilson, T. W., Ladino, L. A., Alpert, P. A., Breckels, M. N., Brooks, I. M., Browse, J., Burrows, S. M., Carslaw, K. S., Huffman,  
651 J. A., Judd, C., Kilhau, W. P., Mason, R. H., McFiggans, G., Miller, L. A., Najera, J. J., Polishchuk, E., Rae, S., Schiller,  
652 C. L., Si, M., Temprado, J. V., Whale, T. F., Wong, J. P. S., Wurl, O., Yakobi-Hancock, J. D., Abbatt, J. P. D., Aller, J.  
653 Y., Bertram, A. K., Knopf, D. A., and Murray, B. J.: A marine biogenic source of atmospheric ice-nucleating particles,  
654 *Nature*, 525, 234-+, 10.1038/nature14986, 2015.

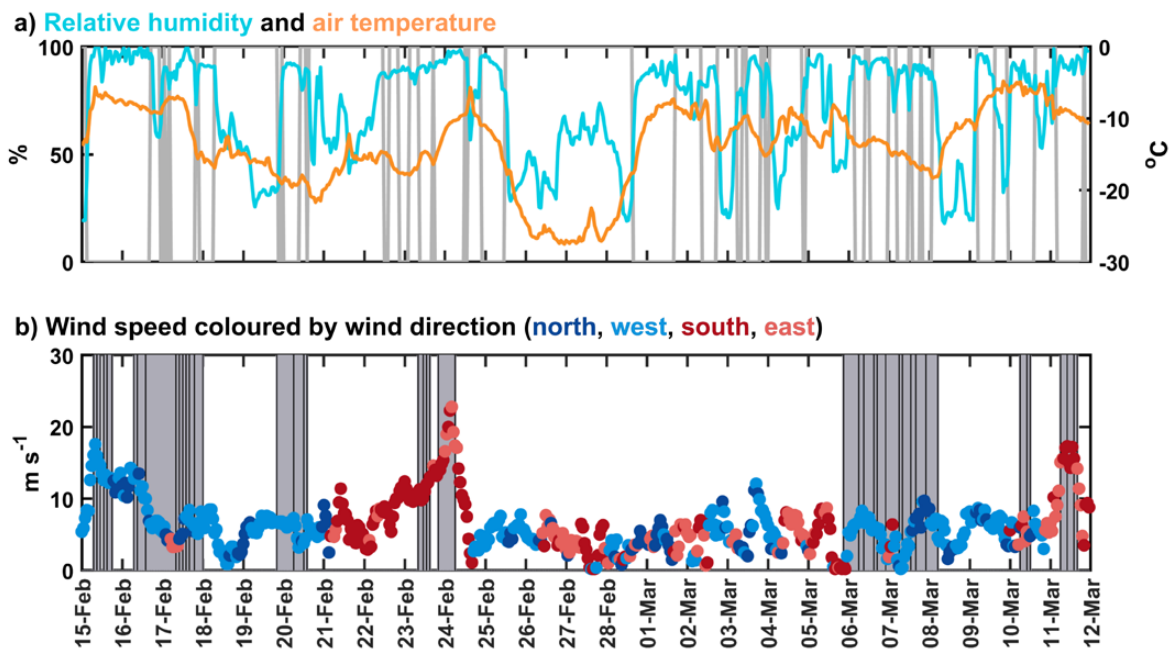


655 Wright, T. P., and Petters, M. D.: The role of time in heterogeneous freezing nucleation, *J Geophys Res-Atmos*, 118, 3731-3743,  
656 10.1002/jgrd.50365, 2013.

657

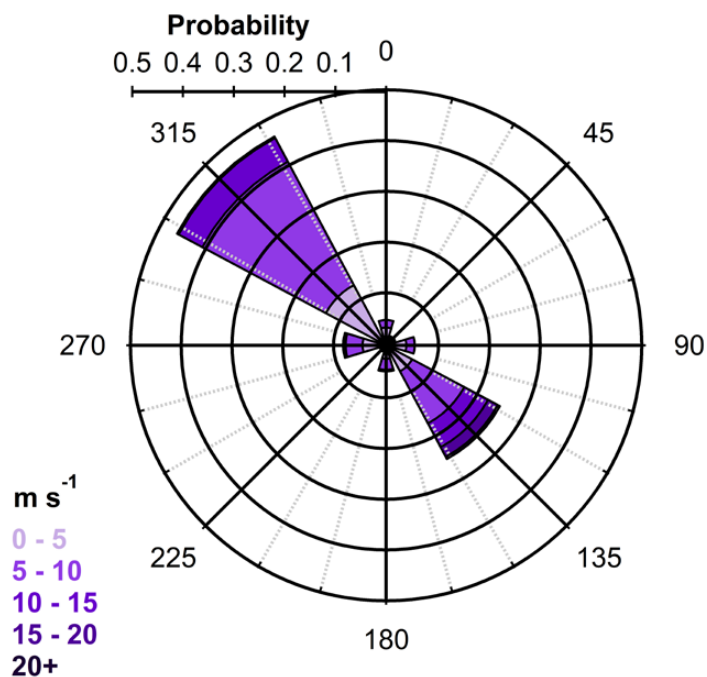

 658 **Table 1. Dates and times for cloud rime, snow, and aerosol samples collected during the 2018 winter INCAS study at Jungfraujoch.**  
 659 **Samples highlighted in blue and red are the northwest and southeast case studies, respectively.**

Date	Cloud rime			Snow			Aerosol			
	Sample	Start (UTC)	Duration (hh:mm)	Sample	Start (UTC)	Duration (hh:mm)	Sample	Start (UTC)	Duration (hh:mm)	Stages
15-Feb	Rime1	06:30	03:07	Snow1	07:15	01:15	DRUM1	10:00	12:00	A/B/C/D
	Rime2	09:37	02:13	Snow2	08:40	01:30	DRUM2	22:00	24:00	A/B/C/D
	Rime3	11:50	03:55	Snow3	10:10	01:35				
	Rime4	15:45	03:35	Snow4	12:45	02:30				
	Rime5	19:20	13:55	Snow5	15:20	04:00				
16-Feb	Rime6	07:15	02:10	Snow6	07:15	02:02	DRUM3	22:00	24:00	A/B/C/D
	Rime7	09:29	02:41	Snow7	09:23	02:37				
				Snow8	14:00	17:50				
17-Feb	Rime8	12:08	01:16	Snow9	07:50	02:23	DRUM4	22:00	24:00	A/B/C/D
	Rime9	13:24	02:23	Snow10	10:16	01:10				
	Rime10	15:47	03:12	Snow11	11:35	00:33				
	Rime11	18:59	06:48	Snow12	12:20	01:04				
				Snow13	13:42	01:00				
				Snow14	14:45	00:55				
18-Feb	Rime12	00:47	08:22	None			DRUM5	22:00	24:00	A/B/C
19-Feb	Rime13	21:00	10:50	Snow17	21:00	08:50	DRUM6	22:00	24:00	A/B/C
20-Feb	Rime14	05:50	04:14	Snow18	05:50	04:14	DRUM7	22:00	24:00	A/B/C
	Rime15	12:08	02:17	Snow19	12:08	02:14				
21-Feb	None			None			DRUM8	22:00	24:00	A/B/C/D
22-Feb	None			None			DRUM9	22:00	24:00	A/B/C/D
23-Feb	Rime16	20:00	14:30	Snow20	07:49	02:51	DRUM10	22:00	24:00	A/B/C/D
				Snow21	10:55	03:35				
				Snow22	14:40	02:42				
				Snow23	20:00	12:11				
24-Feb	None			None			DRUM11	22:00	24:00	A/B/C
25-Feb	None			None			DRUM12	22:00	24:00	A/B
26-Feb	None			None			DRUM13	22:00	24:00	A/B/C
27-Feb	None			None			DRUM14	22:00	24:00	A/B/C
28-Feb	None			None			DRUM15	22:00	24:00	A/B/C
01-Mar	None			None			DRUM16	22:00	24:00	A/B/C
02-Mar	None			None			DRUM17	22:00	24:00	A/B/C
03-Mar	None			None			DRUM18	22:00	24:00	A/B/C
04-Mar	None			None			DRUM19	22:00	24:00	A/B/C
05-Mar	Rime17	16:43	15:32	Snow24	21:52	08:16	DRUM20	22:00	24:00	A/B/C
06-Mar	Rime18	06:15	03:03	Snow25	06:15	02:50	DRUM21	22:00	24:00	A/B/C
	Rime19	09:18	05:42	Snow26	09:14	05:26				
	Rime20	15:00	02:08	Snow27	14:54	01:56				
	Rime21	17:08	04:41	Snow28	17:26	04:04				
	Rime22	22:38	21:40	Snow29	22:38	07:35				
07-Mar	Rime23	06:19	03:58	Snow30	06:19	01:19	DRUM22	22:00	24:00	A/B/C
	Rime24	10:17	05:40	Snow31	07:50	02:00				
	Rime25	15:57	08:31	Snow32	12:49	02:59				
	Rime26	22:28	06:34	Snow33	16:00	05:19				
08-Mar	None			None			DRUM23	22:00	24:00	A/B/C
09-Mar	None			None			DRUM24	22:00	24:00	A/B/C
10-Mar	Rime27	11:00	21:46	Snow35	06:00	04:00	DRUM25	22:00	24:00	A/B/C
				Snow36	10:10	01:56				
11-Mar	Rime28	06:46	02:59	Snow37	05:48	04:03	None			
	Rime29	09:56	03:49	Snow38	09:54	03:51				
	Rime30	13:45	04:48	Snow39	13:48	02:28				



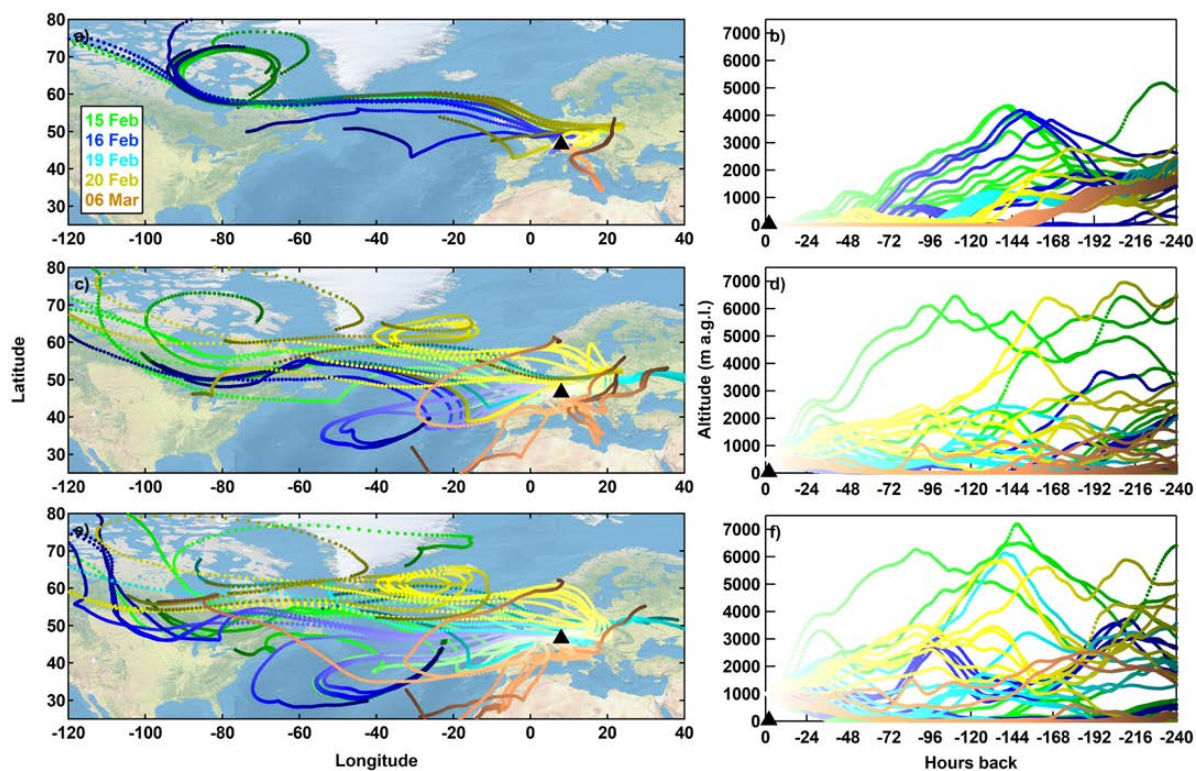
661

662 **Figure 1.** Meteorological data at JFJ from INCAS, including a) relative humidity and surface air temperature and b) wind speed colored  
663 by wind direction. Grey shading in a) indicates in-cloud measurement conditions per the estimation by Herrmann et al. (2015) and in b)  
664 indicates snow and cloud rime collections with the width of the bar indicating the duration of each sample. Aerosol sampling was  
665 conducted daily during all conditions (i.e., precipitation, cloudy, and clear sky). North, east, south, and west correspond to wind direction  
666 ranges of 315 – 45, 45 – 135, 135 – 225, and 225 – 315 degrees, respectively.



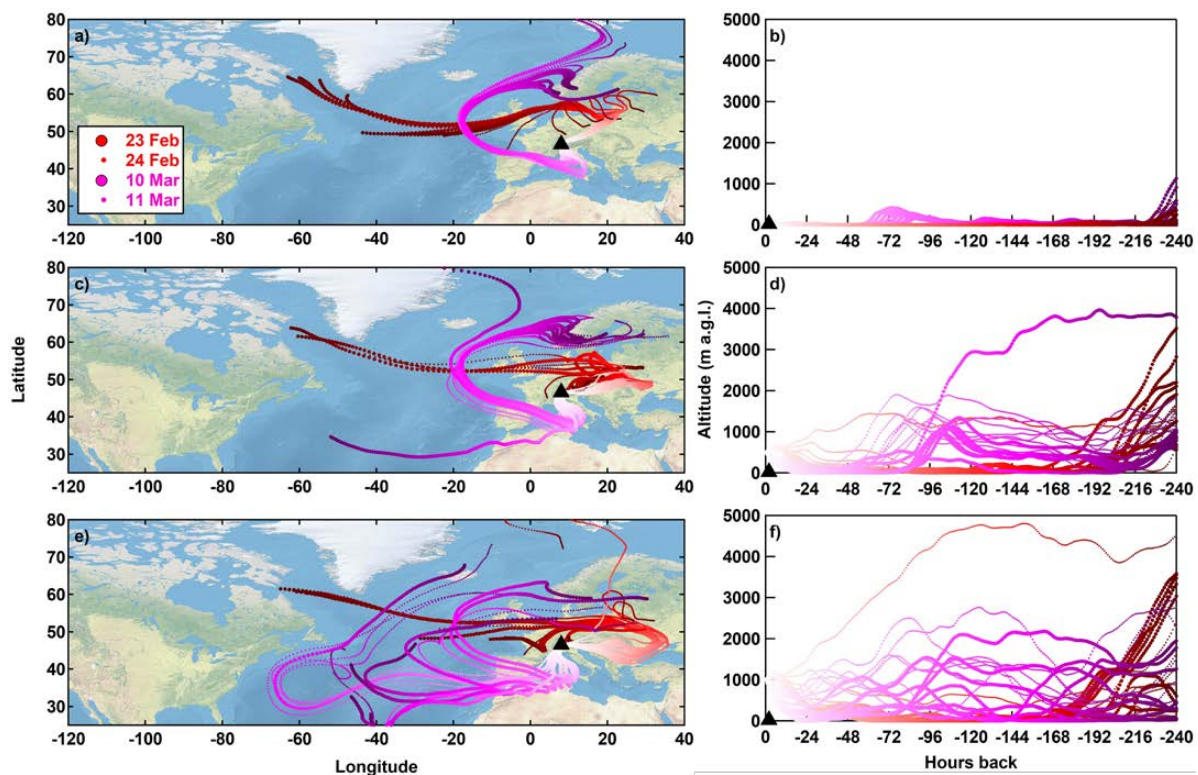
667

668 **Figure 2.** Rose plot for wind data during INCAS. Values correspond to wind direction binned by 45 degrees and wind speeds binned by  
669 **5 m s<sup>-1</sup>. The probability for wind speed to fall within these bins is plotted.**



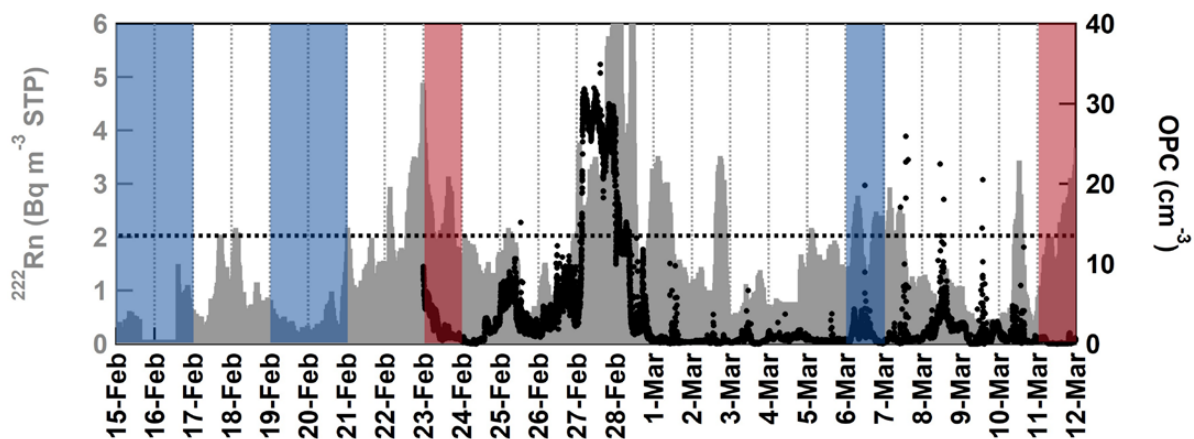
670

671 Figure 3. 10-day air mass backward trajectories initiated every 3 hours during sample collection for northwesterly case days at a) 10, c)  
672 500, and e) 1000 m a.g.l. Altitude profiles versus time are also shown for b) 10, d) 500, and f) 1000 m a.g.l. Each day is coloured  
673 to differentiate between the days.



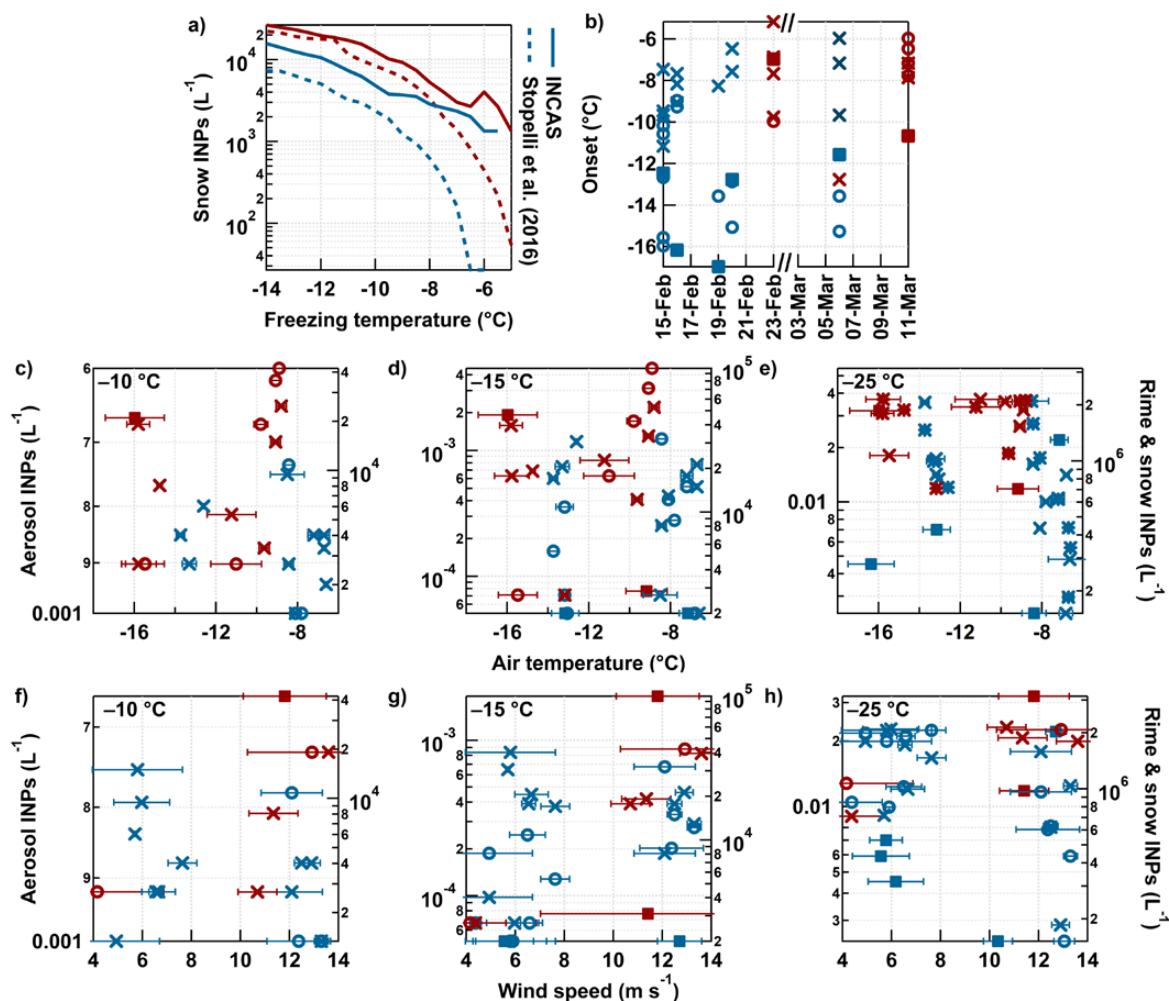
674

675 **Figure 4.** Same as Figure 3, but for southeasterly case days. 24 Feb and 10 Mar are shown as smaller markers, indicative of possible  
676 Saharan dust events from Paul Scherrer Institute.



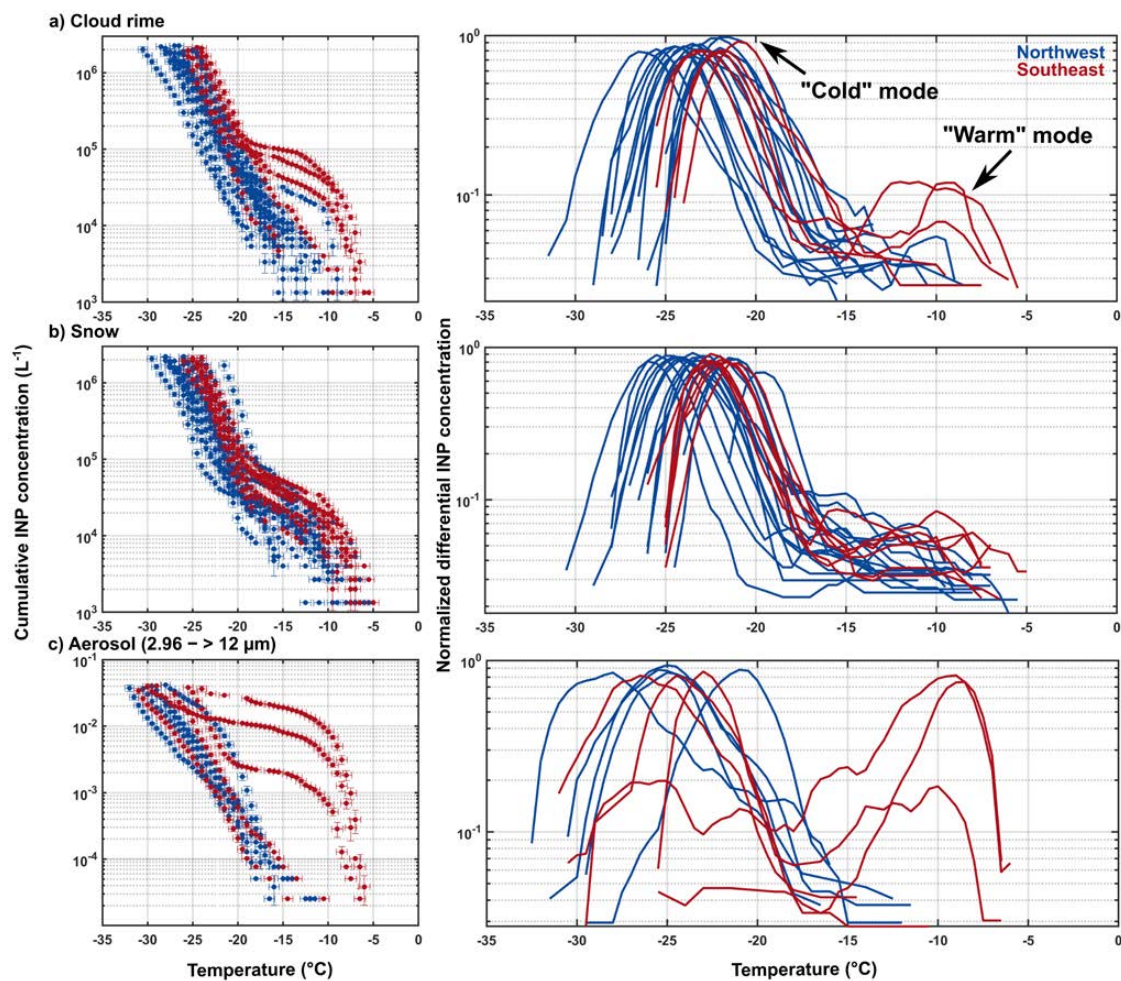
677  
678  
679  
680  
681

Figure 5.  $^{222}\text{Rn}$  concentrations (grey) measured and corrected for standard temperature and pressure during INCAS. OPC particle number concentrations (black) are also shown, but data were missing prior to 23 Feb. The black dashed line indicates a threshold of  $2 \text{ Bq m}^{-3}$  whereby boundary layer intrusion likely occurred at JFJ. Blue and red shadings represent northwesterly and southeasterly case study days, respectively.



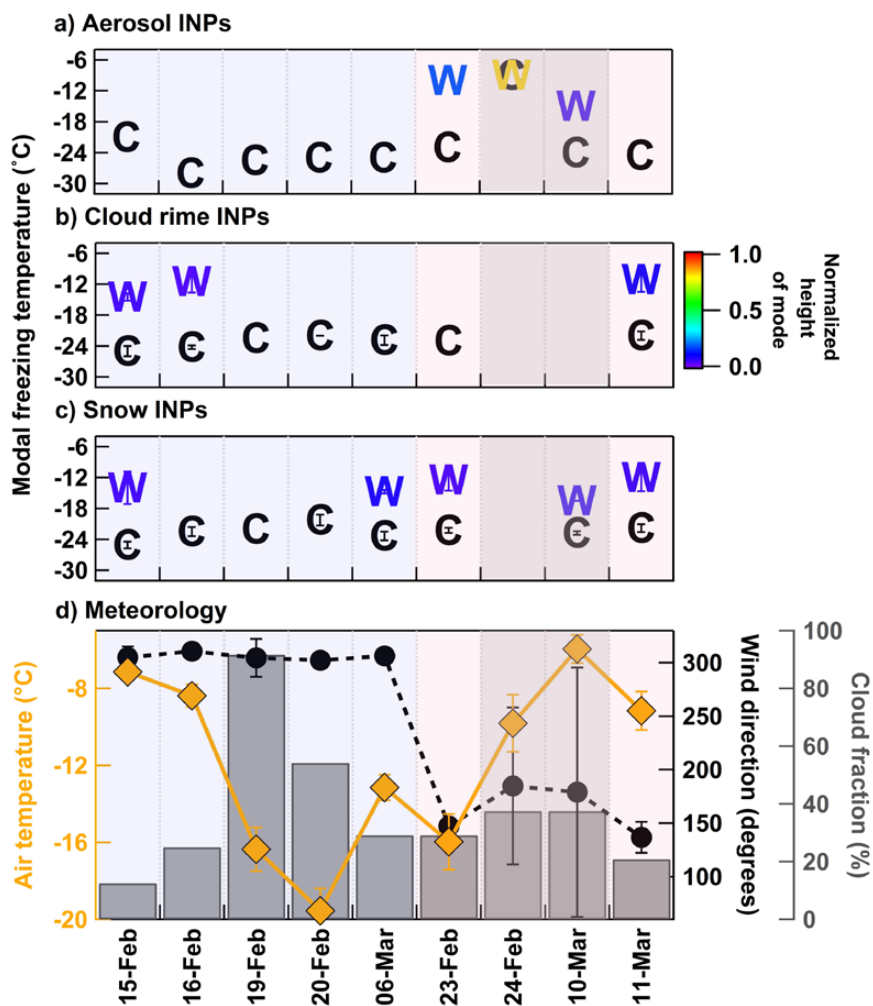
682

683 Figure 6. a) Comparison of INCAS snow INPs within the same range of those reported by Stopelli et al. (2016) for measurements at JFJ  
 684 during the 2012/13 winter season. Summary of INCAS INP concentrations from aerosol (squares), cloud rime (open circles), and snow  
 685 samples (x's), including b) freezing onset temperatures, and correlations between air temperature averages during sample collection and  
 686 INPs at freezing temperatures of c) -10 °C, d) -15 °C, and e) -25 °C. The same concentrations at f) -10 °C, g) -15 °C, and h) -25 °C are  
 687 plotted against average wind speed measured during sample collection periods. Blue and red markers represent northwesterly and  
 688 southeasterly wind directions, respectively.



689

690 Figure 7. Cumulative INP spectra (left) and normalize INP spectra (right) for the same samples of a) cloud rime, b) snow  
691 for the size range  $2.96 - >12 \mu\text{m}$  in diameter. Spectra shown are for samples from the northwest (blue) and southeast (red) case study  
692 dates. Multiple cloud rime and snow samples were collected while one aerosol sample from each size range was collected on case study  
693 days (see Table 1). Additional dates with only aerosol samples (24-Feb and 27-Feb) are also shown in c) (highest of the two modes  $> -15$   
694 °C) and are discussed in section 3.3. The “cold” and “warm” modes are indicated in the normalize INP spectra for cloud rime, for  
695 reference.



696

697 **Figure 8.** Spectral statistics of cold mode height temperature and warm mode height temperatures denoted by “C” and “W”, respectively  
 698 for a)  $2.96 - > 12 \mu\text{m}$  aerosol, b) cloud rime averaged per day, and c) snow averaged per day. Days with only “C” marker indicate the  
 699 absence of a warm mode. d) shows average air temperature, wind direction, and cloud fraction during the case study days. The days are  
 700 ordered by northwesterly (blue shading) and southeasterly (pink shading) case days. The southeasterly cases shaded in grey represent  
 701 days that were not case study days, but days that help explain circumstances of the sampling on 23 Feb and 11 Mar.